Chemical Physics Reviews

REVIEW ARTICLE | NOVEMBER 08 2022

Sensitized triplet–triplet annihilation based photon upconversion in full organic and hybrid multicomponent systems

Alessandra Ronchi ; Angelo Monguzzi

Chem. Phys. Rev. 3, 041301 (2022)
https://doi.org/10.1063/5.0112032

Chemical Physics Reviews REVIEW scitation.org/journal/cpr

Sensitized triplet–triplet annihilation based photon upconversion in full organic and hybrid multicomponent systems

Cite as: Chem. Phys. Rev. 3, 041301 (2022); doi: 10.1063/5.0112032
Submitted: 20 July 2022 · Accepted: 13 October 2022 ·
Published Online: 8 November 2022

View Online Export Citation CrossMark

Alessandra Ronchi and Angelo Monguzzi[a)]

AFFILIATIONS

Dipartimento di Scienza dei Materiali, Università degli Studi Milano-Bicocca, via R. Cozzi 55, 20125 Milano, Italy

[a)]Author to whom correspondence should be addressed: angelo.monguzzi@unimib.it

ABSTRACT

In the last 15 years, the attention dedicated to organic conjugated systems experienced outstanding growth because of the renewed interest in mechanisms involving triplet states such as singlet fission, thermally activated delayed fluorescence, and intersystem crossing enhanced phosphorescence. Photon upconversion via sensitized triplet–triplet annihilation (*s*TTA) enables the conversion of low-energy photons into high-energy ones, and it has been proposed in multicomponent systems as an efficient managing strategy of non-coherent photons. This mechanism exploits the annihilation of two optically dark triplet states of emitter moieties to produce high-energy photons. The annihilating triplets are sensitized through Dexter energy transfer by a light-harvester, typically a conjugated molecule or a nanocrystal, so *s*TTA upconversion is usually performed in bi-component systems. The high yield observed at low excitation intensities stimulated thriving research in the field, leading to the development of a large family of fully organic and hybrid *s*TTA multicomponent upconverters. Here, we compare the evolution of these two families of systems with respect to the *s*TTA upconversion main figures of merit, highlighting the strengths and weaknesses of both approaches, according to the results reported in the literature. The data presented are also discussed in the perspective of future developments in the field, pointing out the challenges that are still to be faced for the technological use of the *s*TTA upconversion process.

I. INTRODUCTION

The annihilation of triplet excitons (TTA) upon collision is a well-known bimolecular process that can be observed in principle in every semiconductor system where the triplets' density and their diffusion ability set a non-negligible encounter probability during their lifetime.[1,2] The output of this interaction can be various. The collisional complex formed by combining two triplet wavefunctions can be indeed represented as a combination of singlet, triplet, and quintet states;[3–5] thus, three main output scenarios can be envisaged, according to the electronic structure energetics of the system considered. Let us consider that the collisional complex has a total energy equal to twice that of the annihilating triplet T_1, namely, $E(T_1)$. If the total energy (electronic plus thermal) of the complex $2E(T_1) + k_B\mathbf{T} \geq E(T_n)$, where T_n is a generic high energy triplet state, the annihilation can be seen as an inelastic process where, in the best case, the collisional complex relaxes to the resonant T_n state that quickly recombines to T_1. In this case, the total energy of half of the initial T_1 state population is lost. This mechanism is common in devices where large populations of triplets are involved such as phosphorescent OLEDs, where it represents a detrimental competitive mechanism for energy dissipation.[6] On the contrary, if $2E(T_1) + k_B\mathbf{T} \geq E(S_n)$, high energy singlet states S_n can be populated from the collisional bimolecular complex. A particularly interesting case is when $2E(T_1) + k_B\mathbf{T} \geq E(S_1)$, i.e., when the TTA mechanism can directly populate the fluorescent S_1 state. The process can be efficient enough to produce an intense delayed fluorescence, whose spectral features match those of prompt fluorescence, while its apparent lifetime is orders of magnitude longer because long living triplets are involved to produce the emissive electronic excited states.[1,2] Thus, the study of this delayed fluorescence is a powerful tool to investigate molecular excitons and TTA physics in molecular semiconductors, given the intrinsic difficulty to interact directly with optically dark triplets, as demonstrated by several seminal works,[5,7,8] and recent literature.[9,10]

Around 2005, Castellano and Baluschev groups[11,12] renovated the attention dedicated to the TTA process by coupling an annihilator moiety with suitable triplet sensitizers in low viscosity solutions,

as shown in Fig. 1. The triplet sensitizers originally employed were organic compounds with strong absorption and fast intersystem crossing (ISC) to populate their own triplets. From these, the energy is transferred to the annihilator triplets through Dexter energy transfer. For well-matched chromophore pairs in low viscosity solvents, the sensitized TTA-based upconversion process (*s*TTA upconversion) shows an excellent yield, which, calculated as the ratio between the number of emitted photons and the absorbed ones, can surpass 30%—close to the upper limit of 50%, see below—under low excitation intensities comparable to the solar irradiance.[13] Because the process can be efficient also under non-coherent light, *s*TTA upconversion can potentially surpass the limitations of traditional photon upconversion mechanisms, such as two-photon absorption or sequential excited state absorption (ESA),[14–16] that require coherent and/or high-intensity radiation to be efficient.[17,18] Therefore, *s*TTA upconversion has been and is still intensively investigated for solar technologies,[19–22] low power bio-imaging,[23,24] optogenetics,[25] anti-counterfeiting,[26] and oxygen sensing applications.[27] Moreover, to overcome some of the limits of fully organic systems, recently the research has started to focus on the development of hybrid *s*TTA systems. In this case, the light-harvesting compound is substituted with a semiconductor nanocrystal, whose energy gap can be more easily tuned for a finer coupling with the annihilator triplets' energies and can cover a larger part of the solar emission spectrum.[28–31] As shown in Fig. 2, in this case, the process photophysics is more complex, because an additional energy transfer step is required to transport the absorbed energy from the semiconductor to the annihilator species, but good results in terms of efficiency have already been obtained.

In this Review, after a short recall of the process kinetics, we compare the evolution of the TTA upconversion systems in the fully organic and hybrid forms with regard to the main figures of merit of the process to highlight the strengths and weaknesses of the two approaches and discuss future developments.

II. KINETICS OF STTA-BASED PHOTON UPCONVERSION

A. Fully organic upconverters kinetics

As shown in Fig. 1, global TTA upconversion or global TTA-UC involves many radiative and non-radiative processes even in the simplest bicomponent fully organic system. Thus, its efficiency depends on the relative yield of all the processes involved in steady state conditions. The time evolution of the molecular excitons populations (both in solution or solid state) can be written as

$$\frac{\partial T_d}{\partial t} = \alpha(\lambda)\phi_{ISC} I_{exc} - k_{fw} T_d - k^0_{T_d} T_d + k_{bk} T_a \tag{1}$$

for the light-harvester and triplet sensitizer energy donor. Here, I_{exc} is the excitation intensity in photons cm^{-2} s^{-1}, $\alpha(\lambda)$ is the absorption coefficient in cm^{-1} at a given wavelength λ, ϕ_{ISC} is the donor intersystem crossing yield, k_{fw} is the forward energy transfer rate constant from donor triplets T_d to acceptor/annihilator triplets T_a, and k_{bk} is the rate constant of the opposite energy transfer process (back-energy transfer). The parameter $k^0_{T_d}$ is the spontaneous decay rate constant of the donor triplets. For the annihilator/acceptor triplets T_a, the differential equation becomes

$$\frac{\partial T_a}{\partial t} = k_{fw} T_d - k^0_{T_a} T_a - k_{bk} T_a - \gamma_{TT} T_a^2, \tag{2}$$

where $k^0_{T_a}$ is the acceptor triplet spontaneous decay rate constant and γ_{TT} is the second order rate constant for the bimolecular TTA process.[1,2] For the emissive acceptor singlet state, i.e., the upconverted electronic state, we can write

$$\frac{\partial S_a}{\partial t} = \frac{1}{2} f \gamma_{TT} T_a^2 - k^0_{S_a} S_a - k^S_{bk} S_a, \tag{3}$$

where $k^0_{S_a}$ is the acceptor singlet spontaneous decay rate constant and k^S_{bk} is the backward energy transfer from the acceptor singlets S_a to the donors.

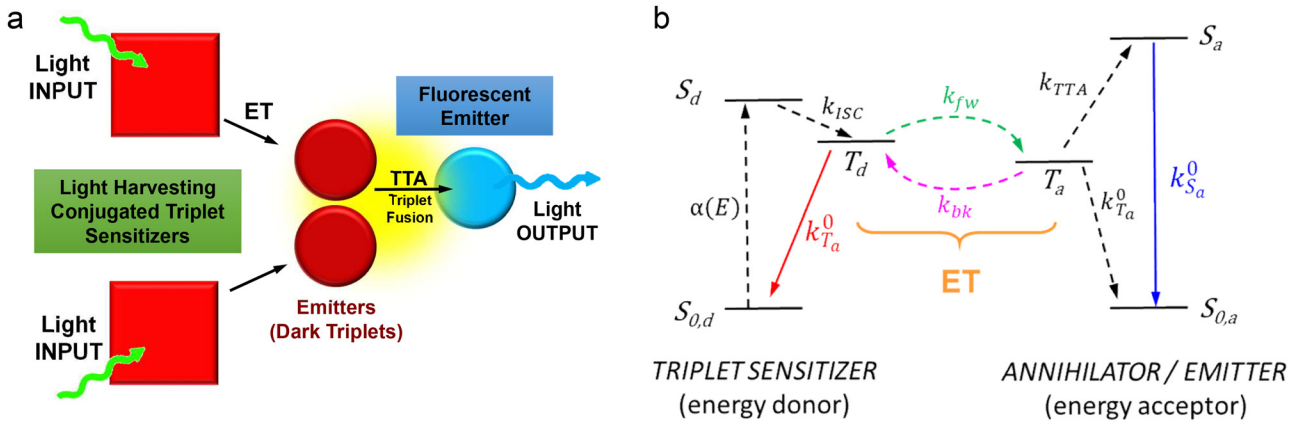

FIG. 1. (a) Sketch of the composition of fully organic *s*TTA upconverting systems, with conjugated molecules working as light-harvesters and sensitizers for the optically dark triplets of a fluorescent dye. (b) Most common sketch of the energy levels involved in the sensitization of the annihilator/emitter triplet states T_a by Dexter energy transfer (ET) from the triplet state T_d of the donor moiety. The light harvester/energy donor, with absorption coefficient $\alpha(\lambda)$, is excited to a singlet state (S_d) that efficiently undergoes intersystem crossing (ISC) to the triplet state T_d. Forward energy transfer occurs with rate k_{fw} and competes with back-energy transfer (k_{bk}) from the acceptor/annihilator triplet T_a. This can either decay spontaneously with rate constant $k^0_{T_a}$ or undergo triplet–triplet annihilation (TTA) with rate constant k_{TTA} to an excited singlet state of the emitter (S_a), generating the high energy fluorescence ($k^0_{S_a}$). The solid lines indicate transitions involving a photon, while the dashed lines refer to radiation-less transitions.

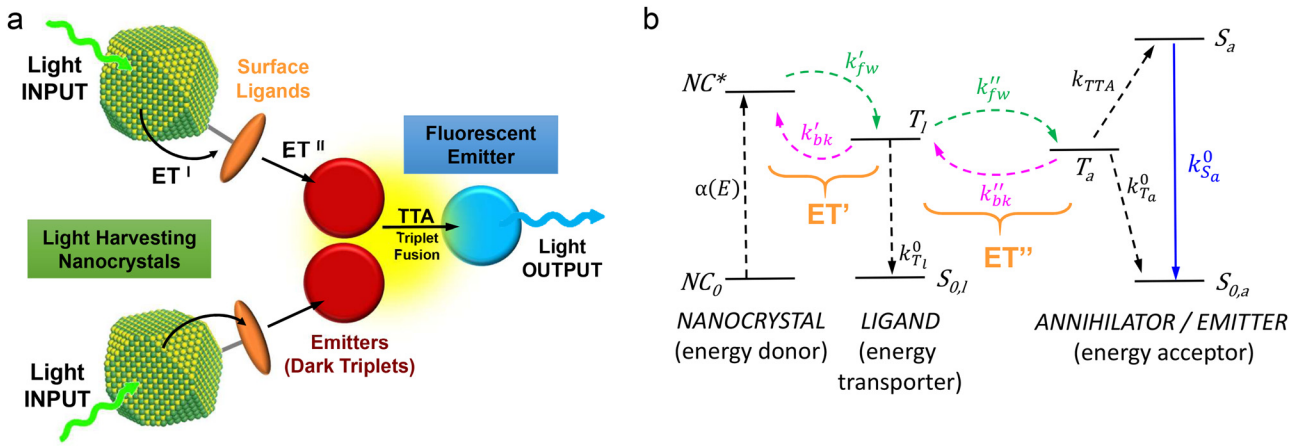

FIG. 2. (a) Sketch of the composition of hybrid molecule–nanocrystal upconverting systems (h-sTTA upconversion), with light-harvesting nanocrystals decorated with conjugated ligands on the surfaces to store the absorbed energy and transfer it to the dark triplets of the fluorescent annihilators. (b) Most common sketch of the energy levels involved in the *s*TTA process in hybrid systems. Upon absorption of a photon, an exciton NC* is created in a nanocrystal. Its energy is transferred via Dexter-type energy transfer (ET^{I}) with rate k'_{fw} to the ligand triplet state T_l, which, in turn, can populate the emitter triplet state T_a through a second transfer (ET^{II}) with rate k''_{fw}. Both transfers must compete with the respective back transfer from the energy acceptor species k'_{bk} and k''_{bk}. As in fully organic upconverters, the annihilation of two encountering emitter triplets (TTA) results in the formation of an emitter high energy excited singlet state S_a from which the upconverted emission is produced. The solid lines indicate transitions involving a photon, while dashed lines refer to radiation-less transitions.

These three correlated differential equations can be solved in the steady state to estimate the TTA-UC yield under a given working condition (i.e., at a given excitation intensity) as a function of intrinsic parameters of the donor/acceptor moieties employed (ϕ_{ISC}, $\alpha(\lambda)$, spontaneous decay rates) and of extrinsic parameters such as the molecular/exciton diffusivity $D(\mathrm{cm}^2\ \mathrm{s}^{-1})$ or the components concentrations. To a first approximation, for high-diffusivity systems such as low viscosity organic solvents,[32–34] the energy transfer rates (k_{fw} and k_{bk}) and the TTA rate ($k_{TTA} = \gamma_{TT} T_a$) depend linearly on the donor (C_d) and acceptor (C_a) concentrations, as well as on the molecular/exciton diffusivities as

$$k_{fw} \propto (D_a + D_d) C_a, \tag{4a}$$

$$k_{bk} \propto (D_a + D_d) C_d, \tag{4b}$$

$$k_{TTA} = \gamma_{TT} T_A \propto D_a T_a. \tag{4c}$$

By solving Eqs. (1) and (2) at a given working condition and knowing the acceptor and donor properties and diffusivities, we can calculate the effective T_a value. This allows us to evaluate directly the TTA rate and yield and consequently, by using Eq. (3), the amount of upconverted singlets generated.[35] In particular, the rate equations system can be solved for simplified limit cases that, as detailed below in Sec. III A, enable to define additional quantitative indicators to evaluate the upconversion performance and, therefore, to draw guidelines to optimize the system composition.

B. Back-energy transfer from annihilator to sensitizers

Equation (4c) shows that the TTA rate is primarily determined by the effective number of triplets available for annihilation. This implies that any mechanism that lowers the T_a value can be seen as a competitive deactivation channel that reduces the global upconversion efficiency. This is the case of the backward energy transfer process from the acceptor to donor triplets.[36] As recently demonstrated,[37] the balance between the forward and backward mechanisms sets the average T_a value that can experience TTA. The relative yields of the energy transfers are given by

$$\phi_{fw} == \frac{k_{fw}}{k_{fw} + k^0_{T_d}}, \tag{5a}$$

$$\phi_{bk} = \frac{k_{bk}}{k_{bk} + k^0_{T_a} + k_{TTA}} \tag{5b}$$

for the forward and backward processes, respectively. Also, it can be demonstrated that under steady state conditions, an asymptotic value for the donor-to-acceptor energy transfer yield ϕ_{ET} can be written as[38]

$$\phi_{ET} = \frac{\phi_{fw}(1 - \phi_{bk})}{1 - \phi_{fw}\phi_{bk}}. \tag{6}$$

This is the limit net transfer efficiency in steady state conditions that should be taken into account to calculate the effective $T_a = \alpha(\lambda)\phi_{ISC}\phi_{ET} I_{exc}$ value. Interestingly, Eq. (6) suggests also a potential strategy to nullify the back-energy transfer negative effect on the TTA-UC, regardless of its efficiency. In fact, both in solution and solid state, the system composition and structure must be tuned to grant ϕ_{fw} as large as 1. In this way, according to Eq. (6), all the excitation energy flows to the acceptor side regardless of the back transfer yield and achieving $\phi_{ET} = 1$, maximizing the number of triplets available for TTA without energy losses at this step.

The second back-energy transfer process in TTA-UC can potentially occur from upconverted acceptor singlets back to the donor singlets. This transfer process has been only barely considered, and its role has not been investigated in detail yet. Despite involving dipole-allowed electronic transitions implying the occurrence of a long range energy transfer process,[1,2] in fully organic upconverters the donor and acceptor systems are usually selected with minimized overlap between

the acceptor fluorescence and the donor absorption spectra to avoid the re-absorption of upconverted photons, allowing to minimize also the k_{bk}^{S} value. Moreover, in model solution systems, the donor absorption is usually quite intense; thus, low C_d values on the order of 10^{-5}–10^{-4} M are required for an adequate material absorptance in 1 cm or even 1 mm thick samples.[39] Consequently, considering the short spontaneous lifetime of the upconverted singlets, the back-transfer probability is quite low, making the process generally negligible. However, when high densities of light-harvesting donors are required in systems showing low exciton mobility, such as in micrometric solid-state devices, the back-energy transfer from upconverted singlets can be in principle a competitive mechanism that should be taken into account to fully model the process kinetics and evaluate its performances.

C. Hybrid upconverters kinetics

All the points discussed so far can be adapted to hybrid systems which, involving a larger number of components with intrinsically different physical properties, are described by a more complex system of rate equations to account also for the role played by the energy bridge ligand that drives the energy from the light harvesting donor nanocrystals to the annihilating moiety. Specifically, we can correlate the fraction of nanocrystals that after the ligand exchange procedure are able to transfer the excitons to the surface ligand triplets (NC^*) and the ligand triplets (T_l) by

$$\frac{\partial NC^*}{\partial t} = \eta\alpha(\lambda)I_{exc} - k'_{fw}NC^* - k^0_{NC}NC^* + k'_{bk}T_l, \tag{7}$$

$$\frac{\partial T_l}{\partial t} = k'_{fw}NC^* - k^0_{l}T_l - k''_{fw}T_l + k''_{bk}T_a. \tag{8}$$

Here, the prime and double prime mark the forward and backward energy transfer process between the excited nanocrystals and the ligand triplets T_l and between the ligand triplets and the acceptor/annihilator triplets T_a, respectively. The most relevant difference with fully organic TTA upconverters is the parameter η introduced in the pump term of Eq. (7). It varies between 0 and 1, and it indicates the fraction of active nanocrystals that participate in the energy transfer process toward the ligand triplets and ultimately populate the acceptor annihilating triplets. In fact, in semiconductor nanocrystals, there are several alternative fast recombination pathways (1–100 ps) absent in conjugated molecules, that, being much faster, can prevent the energy transfer to the ligands. These non-radiative recombination mechanisms that basically switch off instantaneously a fraction of photoexcited nanocrystals can be ascribed to bulk and/or surface electronic impurities and defects that work as traps for the photogenerated electrons and/or holes of the optical excitons.[40] Moreover, the energy-bridge ligands themselves can introduce quenching pathways, as they can act as efficient ultrafast charge scavengers depending on their peculiar electronic structure.[41] Several strategies based on exploiting intermediate electronic states have been proposed to overcome these issues,[41,42] but in any case, the presence of ultrafast quenching mechanisms that limit the population of optically active light harvesting nanocrystals is probably the major bottleneck hindering the global upconversion yield of hybrid TTA upconverters. Once the energy absorbed is funneled into the ligands, we can correlate the populations of annihilator's triplets and singlets by means of two equations similar to those employed for the fully organic system,

$$\frac{\partial T_a}{\partial t} = k''_{fw}T_l - k^0_{T_a}T_a - k''_{bk}T_a - \gamma_{TT}T_a^2, \tag{9}$$

$$\frac{\partial S_a}{\partial t} = \frac{1}{2}f\gamma_{TT}T_a^2 - k^0_{S_a}S_a - k^S_{bk}S_a. \tag{10}$$

Since a two-step energy transfer process is required to sensitize the annihilating triplets in hybrid systems, their effective density can be expressed as $T_a = \eta\alpha(\lambda)\phi'_{ET}\phi''_{ET}I_{exc}$, where ϕ'_{ET} and ϕ''_{ET} are the nanocrystal-to-ligand and ligand-to-annihilator net transfer yields, respectively. It is clear that the full mechanistic picture of the energy flow in hybrid *s*TTA upconverters is definitely more complex than the organic standard.[43–45]

III. STTA UPCONVERSION QUANTITATIVE PARAMETRIZATION

A. TTA excitation threshold

By considering Eqs. (2) and (9), it is clear that at sufficiently high excitation intensities, the TTA rate can outcompete both the back-transfer and spontaneous decay rate of triplets. Under this condition, the TTA is the main recombination channel for the acceptor triplets. Formally, the back-transfer and spontaneous decay rate become negligible, making the TTA yield independent of the excitation intensity and maximized to 1 [*vide infra*, Sec. III B, Eq. (17)], unless other parasitic mechanisms are activated at the powers required to reach this regime.[6,46]

The effective excitation intensity to access the maximum efficiency regime is, therefore, crucial especially for low power applications. In general, any multiphoton process is characterized by an activation excitation regime where the process starts to be efficient. The choice of the efficiency level considered as a target is arbitrary, e.g., 50%, 90%, 95%, etc., since it is a material dependent-empirical parameter. For TTA-based upconverters, the threshold value can be reasonably defined as the intensity at which the TTA rate k_{TTA} equals the sum of the rates of the competitive mechanisms for the annihilator triplets T_a recombination.[35] According to the model discussed above, the use of excitation intensities over a broad range has important consequences on the process global kinetics. Specifically, when using very low excitation intensities, the TTA channel is negligible with respect to the triplet spontaneous decay. Thus, by solving the rate equations system in this limit, i.e., by neglecting the second order term in Eq. (2) [or Eq. (9) for hybrid systems], the emitted upconverted emission intensity shows a quadratic dependence on the excitation intensity I_{exc} consistently with the bimolecular nature of the process. Conversely, in the high excitation regime, the second order term dominates, and all triplets experience TTA. By solving the system neglecting the first order decay term, a linear dependency of the emission intensity vs I_{exc} is found. From these considerations, it follows that the most direct way to evaluate the excitation threshold value is to monitor the emitted upconverted light intensity as a function of the excitation intensity I_{exc} that sets the triplets' density and, therefore, the TTA rate and yield, as shown in Fig. 3(a). The threshold value can be exactly identified as the intersection of the quadratic and linear asymptotic behaviors.

Importantly, the excitation threshold value I_{th}, expressed in ph s^{-1} cm^{-2}, can, in principle, be estimated *a priori* by considering the intrinsic characteristic parameters of the species involved and of the surrounding environment. Specifically, I_{th} can be calculated as[35]

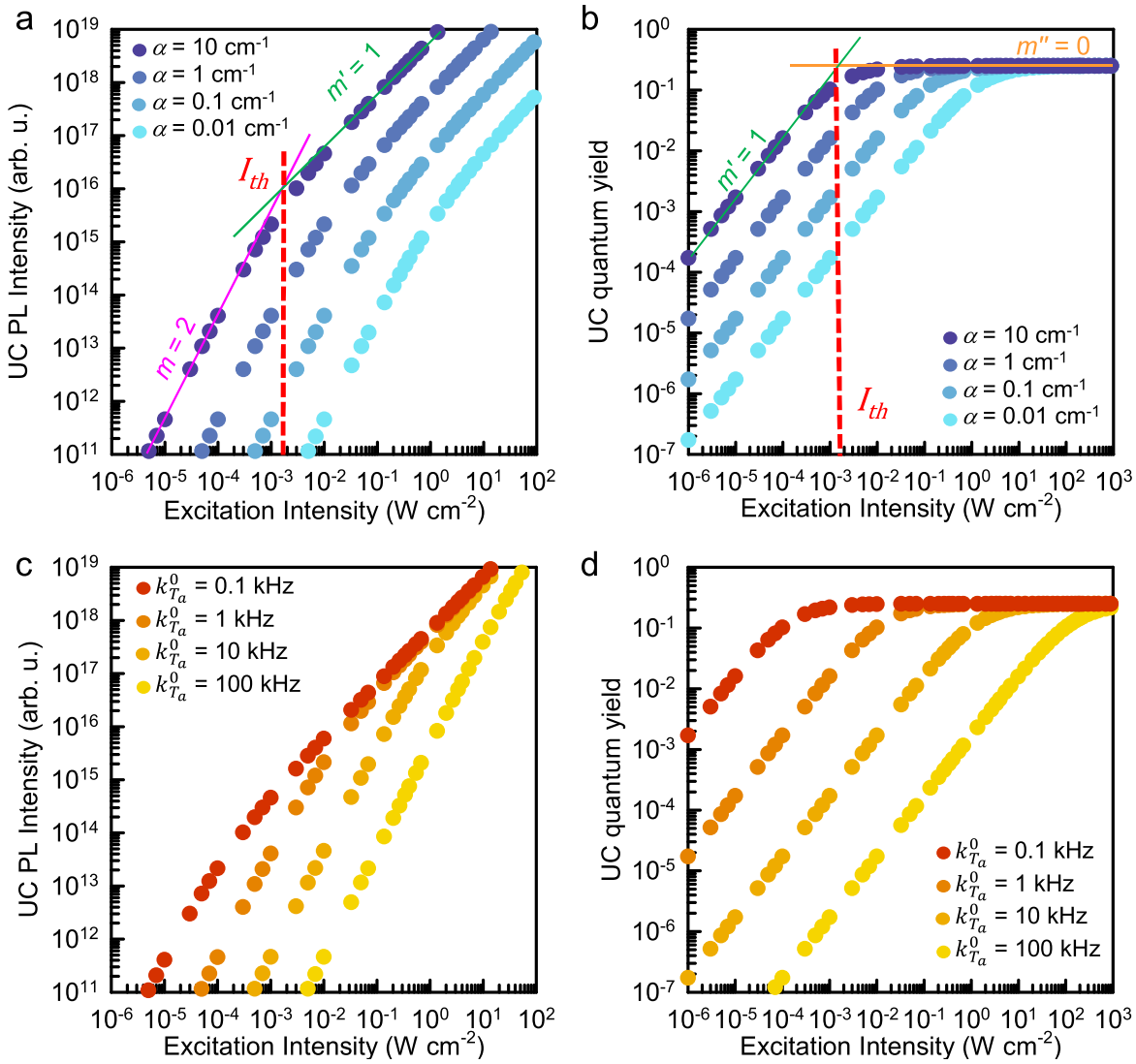

FIG. 3. Upconverted emission (UC PL) intensity as a function of the excitation intensity calculated for different absorption coefficient values α (cm^{-1}) at the excitation wavelength (a) and annihilating triplets' spontaneous decay rate $k_{T_a}^0$ (Hz) (c) for a model system in low viscosity solution. Panel (b) and (d) show the corresponding *s*TTA upconversion quantum efficiency as calculated from Eq. (15). Vertical lines mark the excitation threshold values as defined by Eq. (11).

$$I_{th} = \frac{\left(k_{T_a}^0\right)^2}{\eta\alpha(\lambda)\phi_{ET}\gamma_{TT}}, \tag{11}$$

where $k_{T_a}^0$ is the spontaneous decay rate constant of the annihilator triplets. The parameter $\eta = 1$ in the fully organic case, while $\phi_{ET} = \phi'_{ET}\phi''_{ET}$ for hybrid materials. Equation (11) is useful to (i) reliably estimate the order of magnitude of the threshold value and (ii) point out which parameter has to be optimized to minimize the threshold value. In this regard, Figs. 3(a) and 3(c) illustrate how changing the absorption coefficient and the triplet spontaneous decay rate affects the system performance under different powers, resulting in different threshold values. It is clear how the variation of $k_{T_a}^0$ affects more significantly the threshold because of the quadratic dependence highlighted in Eq. (11). We would like to remind that Eq. (11) derives from a simplified solution of the *s*TTA upconversion kinetics described by Eqs. (7)–(10). More recent and more detailed analysis of the problem led to a particular derivation of the excitation intensity threshold, which can be slightly different if referred to the measurement of the quadratic-to-linear light output behavior discussed above or to the measure of the excitation dependent upconversion yield (*vide infra*). However, we believe that the proposed result is still a fundamental figure of merit for the process, especially considering the typical uncertainty associated with the power-dependent measurements required to evaluate experimentally the excitation threshold.[47]

Tables I–V report the threshold values recorded for several fully organic and hybrid upconverters from 2005 to 2022. Effective *s*TTA

TABLE I. Fully organic *s*TTA upconverters from 2005 to date. The asterisk * marks the upconversion quantum yield Φ_{uc} whose values are reported multiplied by a factor 0.5 to be consistent with the energy conservation law. The double asterisk ** marks the yield values taken from papers where it is not specified if the efficiency is reported as normalized to 1 or not.

Sensitizer	Annihilator	Environment	I_{th} (mW cm^{-2}) (λ_{exc})	Φ_{uc}	ΔE (eV)	Spectral working range	Reference
$[Ru(dmb)_3]^{2+}$	DPA	Organic solvent	−(514.5 nm)	···	0.38	Vis–vis	11
$Ir(ppy)_3$	Pyrene	Organic solvent	−(450 nm)	···	0.42	Vis–uv	105
$PdPh_4OMe_8TNP$	Bis(tetracene)	Organic solvent	−(695 nm)	0.02**	0.71	Vis–vis	106
$PdPh_4MeO_8TNP$	Rubrene	Organic solvent	−(695 nm)	···	0.43	Vis–vis	107
$PdPh_4TBP$	Rubrene	Organic solvent	−(635 nm)	···	0.26	Vis–vis	107
PdTAP	Rubrene	Organic solvent	∼100 (785 nm)	0.01	0.6	Nir–vis	108
$PdPc(OBu)_8$	Rubrene	Organic solvent	−(725 nm)	···	0.5	Nir–vis	109
$PdPh_4TBP$	BPEA	Organic solvent	−(635 nm, working under 70 mW cm^{-2})	0.03	0.58	Vis–vis	110
PtTPBP	Bodipy derivative	Organic solvent	−(635 nm)	0.03**	0.4	Vis–vis	111
PtTPBP	2CBPEA	Organic solvent	−(635 nm)	···	0.58	Vis–vis	112
ZnTPP	Perylene	Organic solvent	−(532 nm)	···	0.48	Vis–vis	113
PtTPBP	Perylene	Organic solvent	−(635 nm)	0.007	0.8	Vis–vis	114
Pyr_1RuPZn_2	N,N-bis(ethylpropyl)-perylene-3,4,9,10-tetracarboxylicdiimid	Organic solvent	−(780 nm)	0.004*	0.7	Nir–vis	115
PtOEP	N,N-bis(ethylpropyl)-perylene-3,4,9,10-tetracarboxylicdiimid	2 POSS-core dendrimers	−(537 nm)	0.002* in DMSO	0.79	Vis–violet	116
Ruthenium(II) polyimine	DPA	Organic solvent	−(473 nm)	0.05*	0.48	Vis–vis	117
PtOEP	DPA	Organic solvent	∼0.3 (532 nm)	0.26	0.52	Vis–vis	38
PdOEP	DPA	Organic solvent	−(514.5 nm)	0.18*	0.46	Vis–vis	118
PdOEP	DPA	Clear Flex 50 film	∼20 (514.5 nm)	0.11*	0.47	Vis–vis	119
PtOEP	DPA	Polystyrene NPs in aqueous suspension	5.6 (532 nm)	0.04	0.52	Vis–vis	120
Bodipy derivative	Perylene	Organic solvent	−(532 nm)	0.08*	0.46	Vis–vis	121
Naphthalenediimide derivative	Perylene	Organic solvent	−(532 nm, working under 10s mW cm^{-2})	0.09*	0.49	Vis–vis	122
PtTPBP	BPEA	ETPTA shell in film	−(633 nm) working under 0.165 mW cm^{-2} at ∼620 nm	···	0.47	Vis–vis	123
PtTPTNP	Perylenediimide	Organic solvent	−(690 nm)	0.03*	0.34	Vis–vis	124
PtTPTNP	Rubrene	Organic solvent	−(690 nm)	0.03*	0.46	Vis–vis	124
Ir-2	DPA	Organic solvent	−(473 nm)	0.12*	0.4	Vis–vis	125
Branched alkyl chain-modified PtOEP	Branched alkyl chain-modified DPA	Solvent free	∼50 (532 nm)	0.14*	0.47	Vis–vis	126
PdTPB	Dye550	PMMA nanocapsules in PVA nanofibers, water dispersion	−(532 nm)	···	0.38	Vis–vis	127
PtOEP	DPA	Poly(butyl acrilate) elastomers	4.3 (532 nm)	0.17	0.52	Vis–vis	128

TABLE I. (*Continued.*)

Sensitizer	Annihilator	Environment	I_{th} (mW cm^{-2}) (λ_{exc})	Φ_{uc}	ΔE (eV)	Spectral working range	Reference
PtTPBP	BDPPA	Polyurethane film	∼80 (635 nm, in toluene) ∼120 (635 nm, in film)	0.09 in toluene solution 0.032 in film	0.69	Vis–vis	129
ZnTPTBP	Perylene-Bodipy dyad	Organic solvent	−(654 nm)	0.004*	0.38	Vis–vis	130
Au (III) complex	DPA	Organic solvent	−(476 nm)	0.10**	0.42	Vis–vis	131
$Ir(C6)_2(acac)$	BDP	Organic solvent	0.78 (445 nm)	0.01	0.52	Vis–uv	132
Cd(II) texaphyrin	Rubrene	Organic solvent	$\sim 1 \times 10^3$ (750 nm)	0.008*	0.56	Nir–vis	133
PdBrTPP	DPA	Organic solvent	−(532 nm, working under 30 mW cm^{-2})	0.18*	0.51	Vis–vis	134
PtTPBP	Perylene	MO/PIB core/ETPTA shell microcapsules in water	130 (635 nm, in MO/PIB)	0.03 in MO/PIB	0.87	Vis–vis	135
IrFppy-pyr	DBP	Organic solvent	−(450 nm)	0.04**	0.53	Vis–uv	136
PdOEP	Poly(DPAMA-co-MMA)	Film	−(543 nm, working under 32 mW cm^{-2})	⋯	0.53	Vis–vis	137
Pd1N3BP + Pd2N2BP + Pd3N1BP + PdTBP + PdTNP	9(10)-Bis(3,3-dimethylbutyn-1yl) perylene	HD core of nanocellulose-based capsules embedded in a cellulose nano-fibers matrix	−(639 nm)	0.08**	0.61	Vis–vis	138
PdNac	Terrylenediimide derivative	Organic solvent	30×10^3 (856 nm)	7×10^{-4}	0.35	Nir–vis	139
PtTPTBPF + PdDBA + Pt1N	Perylene	Organic solvent	0.9 sun ($\lambda_{exc} > 540$ nm)	0.21 0.1 under 1 sun	⋯	Vis–vis	140
$PdPh_4TBP$	Perylene	Organic solvent	∼20 (635 nm)	0.38 0.1 under 1 sun	0.74	Vis–vis	56
$[Cu(dsbtmp)_2](PF_6)$	DPA	Organic solvent	∼100 (488 nm)	0.09*	0.45	Vis–vis	141
PtOEP	Poly(AnMMA-co-MMA)	Organic solvent	∼160 (532 nm)	0.004*	0.77	Vis–vis	142
Pt–DPA dendrimer	DPA-OH dendrimer	Organic solvent	−(473 nm)	0.001*	0.37	Vis–vis	143
PtOEP	Amphiphilic acceptor based on DPA	Organic solvent	8.9 (532 nm)	0.30	0.55	Vis–vis	144
PtOEP	Ionic liquid based on DPA	Solvent free	3 (532 nm)	0.06	0.42	Vis–vis	145
PtOEP	DPA	Gel matrix (LBG) in DMF	1.48 (532 nm)	0.03	0.49	Vis–vis	146
$PdPc(OBu)_8$	Rubrene	Gel matrix (LBG) in DMF	20 (730 nm)	⋯	0.48	Nir–vis	146
PtTPBP	BPEA	Gel matrix (LBG) in DMF	4.1 (635 nm)	⋯	0.49	Vis–vis	146
$Ir(C6)_2(acac)$	DBP	Gel matrix (LBG) in DMF	28 (445 nm)	⋯	0.5	Vis–uv	146
Pd(II) mesoporphyrin IX	DPA	Cross-linked PVOH–HMDI/DMF/DMSO organogels	∼100 (543 nm)	∼0.14	0.53	Vis–vis	147

TABLE I. (*Continued.*)

Sensitizer	Annihilator	Environment	I_{th} (mW cm^{-2}) (λ_{exc})	Φ_{uc}	ΔE (eV)	Spectral working range	Reference
PtP4COONa	Amphiphilic acceptor based on DPA	Water	130 (515 nm)	0.07*	0.35	Vis–vis	148
Pd(II) mesoporphyrin IX	$[Zn(adb)(DEF)2]_n$	PMMA	0.049 (532 nm, estimated)	0.02	0.69	Vis–vis	149
PtOEP	DPA	Polyoctyl acrylate elastomers	0.3 (532 nm)	0.12 under 1 sun 0.21 under 50 suns	0.54	Vis–vis	150
a. PdPc-o-Cou b. PtPc-o-Cou	Rubrene	Organic solvent	a. 17.7 (663 nm) b. 12.8 (663 nm)	a. 0.03* b. 0.01*	0.31	Vis–vis	151
Pd(II) 5,15-diphenyl-0,20-di(4-carboxyphenyl) porphyrin MOF	Zn^{2+} ions + 4,4′-(anthracene-9,10-diyl)-dibenzoate MOF	Solid state	0.85 (532 nm)	<0.001	0.36	Vis–vis	82
Ir(III) complex	DPA	Organic solvent	−(473 nm, working under 10s mW cm^{-2})	0.16*	0.4	Vis–vis	152
PtTPBP	BPEA	PEG-200 and OA core/polyurethane shell	∼200 (635 nm)	0.16*	0.69	Vis–vis	153
ZnOEP	DPA (coordinated to ZnOEP)	Organic solvent	∼40 (532 nm)	∼0.20	0.53	Vis–vis	154
$PdPh_4TBP$	Perylene	Ionogel	∼15 (633 nm)	∼0.05*	0.74	Vis–vis	155
PdmPH3PMA	DPA	Poly(DPAMA- *stat* -MA- *stat* -PdmPH3PMA) in water suspension	$\sim 2 \times 10^3$ (532 nm)	⋯	0.36	Vis–vis	156
$Ru(bpy)_3Cl_2$	$AnCO_2^-$	Water	3×10^3 (488 nm)	<0.01	0.6	Vis–uv	157
PdTPBP	BPEA	Core/shell capsules in aqueous phase	−(633 nm, working under 0.5 mW cm^{-2})	0.13*	0.62	Vis–vis	158
PtP and PdP	4,4'- (Anthracene-9,10-diyl)bis(4,1-phenylene) diphosphonic acid	Solid state device	42 (under 1.5AM simulator)	⋯	⋯	⋯	98
PtOEP and PdTPBP	Perylene	Polyurethane films	−(532 + 635 nm)	⋯	⋯	Vis–vis	159
PtOEP	DPA	Poly(octyl acrylate) matrix (device)	0.3 sun (λ_{exc} > 450 nm)	0.21 0.14 under 1 sun	…	…	160
PdPc-o-Cou	Rubrene	Organic solvent	17.7 (633 nm)	0.04*	0.22	Vis–vis	161
PdTPP	DPA	PAAS hydrogel	23.98 (532 nm)	0.03*	0.49	Vis–vis	162
PtOEP	DPA	THF/OA core/silica shell nanocapsules in THF	−(526 nm)	0.3	0.28	Vis–vis	163
PtOEP	DPAS	Gelatin and triton-X 100 hydrogel	65 (532 nm)	0.07*	0.47	Vis–vis	164
Zinc tetraphenyl-porphyrin derivative	TTBPer	Poly(ethylene glycol)200 matrix doped with OA	359 (532 nm)	0.13*	0.36	Vis–vis	165
Pt(II)−salophen	DPA	Organic solvent	167.2 (635 nm)	0.21	1.08	Vis–vis	166

TABLE I. (*Continued.*)

Sensitizer	Annihilator	Environment	I_{th} (mW cm^{-2}) (λ_{exc})	Φ_{uc}	ΔE (eV)	Spectral working range	Reference
complex			2.8 (598 nm)	(635 nm)			
PdPc	DPP	Organic solvent	−(730 nm)	0.02*	0.56	Nir–vis	167
PtEOP	Zn^{2+} ions + 4,4′-(anthracene-9,10-diyl)-dibenzoate MOF	Poly(butylacrylate)	∼0.2 (532 nm)	0.06	0.55	Vis–vis	74
PtEOP	DPA	D-limonene (green solvent)	1.22 (532 nm)	0.07*	0.55	Vis–vis	168
PdTPTAP	Rubrene	Binary solid	115 (785 nm)	0.003*	0.6	Nir–vis	169
Os(atpy)(tbbpy)Cl^+	Rubrene NPs doped with sensitizer and DBP	Film	$\sim 10 \times 10^3$ (938 nm)	0.02*	0.66	Nir–vis	170
PtTNP	Py5—perylene derivate	Organic solvent	40.7 (635 nm)	0.08*	0.4	Vis–vis	171
PdBrTPP	*p*-DHMPA	Organic solvent	29.78 (532 nm)	0.13*	0.53	Vis–vis	172
[Cu(dsbtmp)2]PF_6	Sodium 10-phenyl anthracene-9-carboxylate	CTAB MCs in water	7.73×10^3 (488 nm)	<0.01	0.48	Vis–vis	173
PdPc	Rubrene	Organic solvent	1.9×10^3 (730 nm)	0.06	0.52	Nir–vis	174
PtPc	Rubrene	Organic solvent	11×10^3 (730 nm)	0.05	0.52	Nir–vis	174
PdPc	tBRub	Organic solvent	3.6×10^3 (730 nm)	0.01	0.52	Nir-vis	174
AN-zinc(II) bis(di-pyrrin) complex	Perylene	Organic solvent	−(510 nm)	0.03*	0.32	Vis–vis	175
IrFsppy	NDS	Water	−(447 nm)	$\sim 4 \times 10^{-4}$ *	1.09	Vis–uv	176
$Ir(ppy)_3$	PPOS	Ionic liquid P66614	61 (445 nm)	0.002*	0.49	Vis–uv	177
$Pd(MeTPP)_2$	DPA	Organic solvent	−(532 nm, working under 78 mW cm^{-2})	0.29** (under 78 mWcm^{-2})	0.53	Vis–vis	178
$Zr(^{Mes}PDP^{Ph})_2$	DPA	Organic solvent	13 (514.5 nm)	0.21*	0.66	Vis–vis	179
$PdPc(OBu)_8$	Rubrene doped with DBP	Film	2.3 (726 nm without DBP)	5×10^{-5}	0.33	Nir–vis	180
$Ir(C6)_2(acac)$	TIPS-Nph	Organic solvent	1.1 (445 nm)	0.1*	0.55	Vis–uv	181
PtTPBP	PCP	Organic solvent	1.3×10^3 (635 nm)	0.42	0.71	Vis–vis	182
PdOEP	DPA	Nanostructured polymers	500 (532 nm)	0.23	0.55	Vis–vis	87
$[Mo(L^3)_3]$	DPA	Organic solvent	−(635 nm)	0.02*	0.93	Vis–vis	183
PtOEP	DPAS	Film	14 (532 nm)	0.16	0.51	Vis–vis	184
PdTPP	DPA	PEG200	133 (532 nm)	0.12	0.62	Vis–vis	185
PtOEP	DPBF	Organic solvent and device	92 (532 nm, in solution)	0.16 in solution under 115 mW cm^{-2} 0.19 in OLED under 0.1 mW cm^{-2}	0.23	Vis–vis	186
PQ_4Pd	Perylene	Organic solvent	−(655 nm)	0.3*	0.86	Vis–vis	187

upconversion thresholds lower than 1 mW cm^{-2} have been observed in several systems, demonstrating the suitability of the process to work at intensity levels comparable with the solar irradiance. On the contrary, in hybrid systems, I_{th} reaches values so low only in few cases. Of course, there are less scientific papers focused on hybrid materials available because of their relatively recent appearance, but also I_{th} is seldom reported. Nevertheless, the number of scientific works is continuously growing, so some common guidelines should be taken into

TABLE II. Hybrid *s*TTA upconverters from 2005 to date. The asterisk * marks the upconversion quantum yield Φ_{uc} whose values are reported multiplied by a factor 0.5, to be consistent with the energy conservation law. The double asterisk ** marks the yield values taken from papers where it is not specified if the efficiency is reported as normalized to 1 or not.

Sensitizer light harvester: ligand	Annihilator	Environment	I_{th} (mW cm^{-2}) (λ_{exc})	Φ_{uc}	ΔE (eV)	Spectral working range	Reference
PbS NCs layer	Rubrene layer doped with DBP	Film	a. 12×10^3 (850 nm) b. 17×10^3 (960 nm) c. 26×10^3 (1010 nm)	a. 0.01 b. 0.005 c. 0.002 (808 nm)	a. 0.57 b. 0.73 c. 0.8	Nir–vis	83
PbSe NCs	Rubrene	Organic solvent	$\sim 70 \times 10^3$ (980 nm)	0.005*	0.99	Nir–vis	188
CdSe NCs: 9-ACA	DPA	Organic solvent	−(532 nm)	0.08**	0.69	Vis–vis	189
CdSe/ZnS NCs: 4-(10-phenylanthracene-9-yl)pyridine	DPA	Organic solvent	290 (532 nm)	0.007*	0.5	Vis–vis	190
PbS NCs: CPT	Rubrene	Organic solvent	−(808 nm)	a. 0.009*	0.68	Nir–vis	191
PbSe NCs: CPT	Rubrene	Organic solvent	−(808 nm)	0.01*	0.68	Nir–vis	191
PbS/CdS NCs: 5-CT	Rubrene	Organic solvent	3.2 (808 nm)	0.04*	0.68	Nir–vis	192
CdSe NCs: 9-ACA	DPA	Organic solvent	−(532 nm)	0.07*	0.54	Vis–vis	193
CdS/ZnS NCs	PPO	Organic solvent	$\sim 2 \times 10^3$ (405 nm)	0.03*	0.43	Vis–uv	194
PbS NCs layer	Rubrene layer doped with DBP	Film	−(808 nm)	0.04*	0.5	Nir–vis	195
$CsPbX_3$ (X:Br/I) NCs: AEDPA	DPA	Organic solvent	25 (532 nm)	0.007*	0.53	Vis–vis	196
CdSe/ZnS NCs: 9-ACA	DPA	Organic solvent	−(488 nm)	0.05*	0.34	Vis–vis	197
CdSe/CdS NCs doped in annihilator MOF	4,4′-(anthracene-9,10-diyl) dibenzoate based MOF	Poly(butylacrylate)	10^3 (532 nm)	5×10^{-4}*	0.42	Vis–vis	198
PbS NCs doped in annihilator MOF	Diphenyltetracene-containing MOF	Poly(butylacrylate)	13×10^3 (785 nm)	⋯	0.67	Nir–vis	198
$CsPbBr_3$ NCs: NCA	PPO	Organic solvent	1.9×10^3 (443 nm)	0.05*	0.70	Vis–uv	199
$CsPb(Cl/Br)_3$ NCs: NCA	PPO	Organic solvent	4.7×10^3 (445 nm)	0.02*	0.63	Vis–uv	200
CdSe NCs: 9-ACA	DPA	Organic solvent	4.9×10^3 (532 nm)	0.003	0.55	Vis–vis	201
$CuInS_2$/ZnS NCs: 9-ACA	DPA	Organic solvent	−(520 nm)	0.09*	0.64	Vis–vis	42
PbS NCs: 5-CT	Rubrene	Organic solvent	53.4×10^3 (781 nm)	0.06*	0.63	Nir–vis	30
PbS NCs: TES-ADT	TES-ADT	Organic solvent	$\sim 40 \times 10^3$ (1064 nm)	5×10^{-4}	0.86	Nir–vis	202
CdSe nanoplatelets: 9-ACA	DPA	Organic solvent	237 (532 nm)	0.03*	0.55	Vis–vis	203
Au:CdSe NCs: 9-ACA	DPA	Organic solvent	200 (532 nm, absorbed)	0.12	0.49	Vis–vis	41
Si NCs: 9EA	DPA	Organic solvent	a. 950 (488 nm) b. 2×10^3 (532 nm)	a. 0.04* (488 nm) b. 0.005* (640 nm)	a. 0.48 (488 nm) b. 0.69 (532 nm)	Vis–vis	204
PbS NCs: TTCA	V79 derivative	Organic solvent	−(1140 nm)	0.0003 (808 nm)	0.68	Nir–vis	205
CdSe NCs: 10-Ph-ADP	DPA	Organic solvent	163 (532 nm)	0.08*	0.55	Vis–vis	206
CdSe/ZnS NCs: rhodamine B	DPA	Organic solvent	1.2×10^3 (635 nm)	0.01*	1.13	Vis–vis	207
InP/ZnSe/ZnS NCs: 9-ACA	DPA	Organic solvent	−(590 nm)	0.05*	0.98	Vis–vis	208

TABLE II. (*Continued.*)

Sensitizer light harvester: ligand	Annihilator	Environment	I_{th} (mW cm^{-2}) (λ_{exc})	Φ_{uc}	ΔE (eV)	Spectral working range	Reference
$CsPbBr_3$ NCs: 2-ACA	DPA	Organic solvent	6.9×10^3 (443 nm)	0.07*	0.26	Vis–vis	209
CdSe NCs: 9-ACA	DPA	Organic solvent	−(532 nm)	0.08*	0.55	Vis–vis	210
CdSe NCs	4,4′-(anthracene-9,10-diyl)bis(4,1-phenylene) diphosphonic acid	TTA-UC integrated solar cell	0.9	...	...	...	211
PbS NCs: 5,11-bis(-triethylsilylethynyl) anthradithiophen	5,11-bis(triethyl silyle-thynyl) anthradithiophen	Organic solvent	a. $>130 \times 10^3$ (785 nm) b. $>260 \times 10^3$ (975 nm)	a. 0.002* b. 3×10^{-4}*	a. 0.45 b. 0.76	Nir–vis	212
CdTe nanorods: 9-ACA	DPA	Organic solvent	93 (520 nm)	0.02*	0.5	Vis–vis	213
CdS NCs: 3-PCA	PPO	Organic solvent	950 (405 nm)	0.10*	0.48	Violet–uv	214
$CsPbBr_3$ NCs: PPOS	TIPS-Naph	Organic solvent	1.6×10^3 (515 nm)	7×10^{-5}*	0.9	Vis–uv	215
Si NCs: 9EA	DPA	Organic solvent and P188 MCs in water	−(488 nm)	0.08 in methyl oleate 0.06 in MCs	0.33	Vis–vis	216
ZnSe/ZnS NCs: biphenyl BCA	DTBN	Organic solvent	2.4×10^3 (405 nm)	0.03*	0.8	Violet–UVB	217
ZnSe/ZnS NCs: biphenyl BCA	p-TIPS-B	Organic solvent	−(405 nm)	<0.01	0.93	Violet–UVB	217
$CsPbBr_3$ NCs: 9-phenanthrene carboxylic acid	PPO	Organic solvent	$\sim 2.2 \times 10^3$ (473 nm)	0.02*	0.87	Vis–uv	218
$CsPbBr_3$ NCs: 9-phenanthrene carboxylic acid	PPO	Organic solvent	$\sim 1.6 \times 10^3$ (443 nm)	0.06*	0.69	Vis–uv	218

account for reliable performance estimation and comparison. In this regard, two general comments should be made. First, to compare properly the experimental threshold values, essential details must be reported and correlated among different papers. The most important thing is to point out if the threshold is referred to the incident intensity or to the absorbed intensity. In the first case, the reader should be able to recover the absorption coefficient of the material and in the case of bulky solid upconverters also the optical path to calculate the system absorptance.[48] Second, we would like to emphasize that generally all parameters in Eq. (11) are considered constant. As recently discussed,[49] this assumption may not be valid under particular working conditions, for example, when high excitation intensities are employed, so in these cases, a new method based on time resolved photoluminescence spectroscopy experiments has been proposed. It allows us to take into account the power-dependent effects on the chromophores intrinsic properties and to get rid of the experimental uncertainty on the steady state ϕ_{uc} measurements. Therefore, while Eq. (11) is still a powerful tool to predict or verify the system performance, a more refined evaluation can be now carried out to investigate the photophysics of the *s*TTA upconversion process in both organic and hybrid systems under specific working conditions.

B. Upconversion quantum yield

Photon upconverting materials can be envisaged as apparent anti-Stokes emitters that upon absorption of excitation light show photoluminescence at energy higher than that of the photons absorbed. This behavior can be ascribed to TTA or to many other processes, including phonon absorption, non-linear optical properties, sequential and simultaneous multiple absorptions.[14–16] These mechanisms are extensively studied not only for the general interest in the fundamental physics involved, but also for their potential application. It is important to quantify, for example, the efficiency increment of a solar cell that an upconverter can introduce. Therefore, a rigorous definition and experimental determination of the photon conversion quantum yield ϕ_{uc} are necessary to estimate the amount of upconverted photons produced and, at the same time, to help the scientific readership to move among the growing number of upconverting materials.

TABLE III. *s*TTA upconverters developed for bio-related applications. The asterisk * marks the upconversion quantum yield Φ_{uc} whose values are reported multiplied by a factor 0.5, to be consistent with the energy conservation law. The double asterisk ** marks the yield values taken from papers where it is not specified if the efficiency is reported as normalized to 1 or not. OA: oleic acid, HD: hexadecane, NPs: nanoparticles, and MCs: micelles.

Sensitizer	Annihilator	Environment	Ith (mW cm^{-2}) (λ_{exc})	Φ_{uc}	ΔE (eV)	Spectral working range	Refs.
PdOEP	Perylene	HD core/PSAA shell NPs in aqueous dispersion	−(532 nm)	···	0.49	Vis-vis	219
PdOEP	DPA	Stabilized by Pluronic F127 in silica NPs in aqueous solution	—working under 532 nm 8.5 mW cm^{-2}	0.02*	0.53	Vis–vis	220
PtTPBP	BODIPY derivative	Soybean core/BSA-dextran shell nanocapsules in water	∼40 (635 nm)	0.02*	0.32	Vis–vis	221
PdTBP	Dye550	1-phenyl heptadecane core/ PMMA shell NPs in water dispersion	−(633 nm)	···	0.3	Vis–vis	222
PdOEP	DPA	PLA−PEG MCs in aqueous solution	∼150 (532 nm)	under 150 mW cm^{-2}	0.69	Vis–vis	73
PtOEP	Perylene	Lipidic vesicles in PBS	∼50 (630 nm)	···	0.85	Vis–vis	59
PtTPBP	2,5,8,11-tetra[tert -butyl)perylene	Polymersomes in water dispersion	∼200 (630 nm)	0.002*	0.73	Vis–vis	60
PtOEP	DPA	Kolliphor MCs in aqueous dispersion	<30 (532 nm)	0.07	0.5	Vis–vis	223
PdTPBP	a. Perylene b. BPEA	OA core/silica shell nanocapsules in aqueous suspension	∼170 (635 nm)	a. ∼0.045 b. ∼0.03	a. 0.69 b. 0.46	Vis–vis	224
PdOEP	DPA	Poly(D, L -lactic acid)−poly(ethylene oxide) block copolymer NPs	−(530 nm)	···	···	Vis–vis	225
BDP-F	PEA	Mesoporous silica NPs	19.6 (650 nm)	0.02* in toluene	0.96	Vis–vis	226
a. PtOEP b. PdTPTBP	a. DPA b. Perylene	PEGylated DMPC liposomes in aqueous solution	−(a. 532 nm) −(b. 630 nm)	a. 0.01* b. 0.003*	a. 0.65 b. 0.73	Vis–vis	227
PtTPBP	BDP	BSA-stabilized soybean oil droplets in aqueous solution	−(635 nm)	···	0.27	Vis–vis	228
Pd-TCPP	Zr-MOF based on 4,4′-(9,10-anthracenediyl) dibenzoic acid	Water	2.5 (532 nm)	0.006*	0.49	Vis–vis	24
PtTPBP	BDM	Nujol core/BSA shell NPs in water	65 (635 nm)	0.03**	0.34	Vis–vis	229
$PdPC(OBu)_8$	BPEN	Soybean oil core/BSA film in water	∼400 (730 nm, in soybean oil)	0.006* in soybean oil	0.33	Nir–vis	23
DIBP	Perylene	Silica NPs	−(514 nm)	···	0.28	Vis–vis	230
Lu[III] complex of tetrapentafluorophenyl porphyrin	BPEA	DMF core/PEG400 shell nano-MCs in water	340 (561 nm, in toluene)	0.06* in toluene	0.37	Vis–vis	231
		Mesoporous silica NPs in water		0.007* in MCs 0.01* in NPs			

TABLE III. (*Continued.*)

Sensitizer	Annihilator	Environment	Ith (mW cm^{-2}) (λ_{exc})	Φ_{uc}	ΔE (eV)	Spectral working range	Refs.
PtOEP	Amphiphile based on DPAS	Water	25 (532 nm)	0.004*	0.54	Vis–vis	232
$Os(peptpy)_2^{2+}$	TTBP	Pluronic F127 hydrogels	13×10^3 (724 nm)	<0.001	0.85	Nir–vis	233
PdTPBP	Perylene	OA laden mesoporous silica microcapsules in aqueous suspension	∼100 (635 nm)	0.002*	0.8	Vis–vis	234
PtTPBP	BDTS	BSA nanocapsules in water	∼30 (635 nm)	0.03*	0.22	Vis–vis	235
PtTPTNP	TIPS-An	Hydrogels	−(710 nm)	···	1.01	Vis–vis	236
PdTBP	BDMBP	Rice bran oil core/PMMA shell nanocapsules in aqueous solution	−(633 nm)	···	0.74	Vis–vis	237
PdTPBP	Peryelene	PAA-OA NPs in PBS	138.9 (650 nm)	0.005*	0.79	Vis–vis	27
PdTPBP	BDP	PSMA-PEG-OAm NPs in aqueous solution	46.7 (650 nm, in toluene)	0.04* under 20 mWcm^{-2} in toluene	0.31	Vis–vis	238
PtOEP	p-DHMPA	Pluronic F127 nanoMCs in aqueous suspension	−(532 nm)	0.02*	0.53	Vis–vis	239
PtOEP	DPA	PLGA polymer in water	−(535 nm)	···	0.55	Vis–vis	240

TABLE IV. Biocompatible *s*TTA upconverters. The asterisk * marks the upconversion quantum yield Φ_{uc} whose values are reported multiplied by a factor 0.5, to be consistent with the energy conservation law. The double asterisk ** marks the yield values taken from papers where it is not specified if the efficiency is reported as normalized to 1 or not. HD: hexadecane, NPs: nanoparticles, and MCs: micelles.

Sensitizer	Annihilator	Environment	Ith (mW cm^{-2}) (λ_{exc})	Φ_{uc}	ΔE (eV)	Spectral working range	Refs.
PdTBP	Perylene	PTS MCs in water	<10 (635 nm)	0.02	0.87	Vis–vis	241
PtOEP	DPA	HD/PIB mixture nanocapsules in water	∼200 (532 nm)	0.14*	0.69	Vis–vis	242
$Ru(bpy)_3]^{2+}$	(R)-1-O-[4-(1-pyrenylethynyl)phenylmethyl]glycerol	DNA in aqueous solution	−(500 nm)	···	0.47	Vis–vis	243
PdOEP	Perylene	HD core/polystyrene shell NPs in water	−(532 nm)	···	0.49	Vis–vis	244
PdTPBP	Perylene	Microcapsules in aqueous solution	∼90 (635 nm)	···	0.69	Vis–vis	245
PtOEP	DPA	Poly(ε-caprolactone) end-functionalized with DPA in aqueous dispersion	189 (532 nm)	0.08	0.62	Vis–vis	246
PtOEP	DPA	Fmoc-L_3 amphiphilic peptides in water	16.26 (532 nm)	∼0.03*	0.52	Vis–vis	247

TABLE V. *s*TTA upconverters with unconventional sensitizers, such as TADF molecules, (heavy) metal free compounds, molecules with direct S_0-T_1 absorption. The asterisk * marks the upconversion quantum yield Φ_{uc} whose values are reported multiplied by a factor 0.5, to be consistent with the energy conservation law. The double asterisk ** marks the yield values taken from papers where it is not specified if the efficiency is reported as normalized to 1 or not.

Sensitizer	Annihilator	Environment	Ith [mW cm^{-2}] (λ_{exc})	Φ_{uc}	ΔE (eV)	Spectral working range	Reference.
TIHF	DPA	Organic solvent	−(532 nm)	∼0.006**	0.53	Vis–vis	248
2,3-butanedione	PPO	Organic solvent	−(442 nm)	∼0.006**	0.64	Vis–uv	249
Fullerene C60–bodipy C-2 dyad	Perylene	Organic solvent	−(589 nm)	0.04*	0.65	Vis–vis	68
Ketocoumarin compound	DPA	Organic solvent	−(445 nm)	0.06*	0.24	Vis–vis	69
Pyr_1RuPZn_2	Rubrene	Organic solvent	−(740 nm)	0.03* (680 nm)	0.43	Nir–vis	250
4 CzTPN-Ph	DPA	Organic solvent	−(532 nm)	0.001*	0.55	Vis–vis	62
4CzIPN	p-terphenyl	Organic solvent	$\sim 20 \times 10^3$ (445 nm)	0.01*	0.83	Vis–uv	63
Osmium complex	Rubrene	PVA film	$\sim 10 \times 10^3$ (938 nm)	0.02* (730 nm)	0.82	Nir–vis	66
4CzIPN	p-quarterphenyl	Organic solvent	775 (445 nm)	0.02*	0.73	Vis–uv	63
$Os(bptpy)_2^{2+}$ complex	TTBP	Organic solvent	320 (724 nm)	0.01*	0.97	Nir–vis	251
Bodipy−anthracene dyad	Perylene	Organic solvent	−(510 nm)	0.08* under 50 mWcm^{-2}	0.39	Vis–vis	252
C 60–Bodipy dyad	Perylene	Organic solvent	∼600 (532 nm)	0.04*	0.42	Vis–vis	70
BTZ-DMAC	DPA	Organic solvent	−(532 nm)	0.01*	0.52	Vis–vis	64
a. PdTPBP b. PtTPBP	TIPS-Ac	Organic solvent	a.—(635 nm) b. 400 (785 nm)	a. 0.27 (635 nm) b. 0.04 (635 nm)	a. 0.69 b. 1.03	a. Vis–vis b. Nir–vis	253
4CzPN	DBP	Organic solvent	−(450 nm)	∼0.02*	0.55	Vis–uv	71
DCF-MPYM	DPA	Organic solvent	168.04 (635 nm)	0.06*	0.94	Vis–vis	65
Os(II) complex	DPA	Organic solvent	200 (663 nm)	0.03*	1.14	Vis–vis	67
4CzIPN	Pyrene	Organic solvent	$\sim 2 \times 10^3$ (455 nm)	0.003*	0.36	Vis–uv	254
4CzIPN	p-terphenyl	Organic solvent	−(445 nm)	⋯	0.82	Vis–uv	254
$2PF_2$	Perylene	Organic solvent	−(532 nm)	0.19*	0.49	Vis–vis	255
Bodipy derivative	9-(2-phenylethynyl)-10-[2-(trimethylsilyl)ethynyl] anthracene	Solution	31.6 (561 nm)	0.03**	0.49	Vis–vis	256
$Os(tpy)_2^{2+}$	(i-Pr2 SiH)2An	Organic solvent	$\sim 20 \times 10^3$ (724 nm)	0.06*	1.28	Nir–violet	257
TSQ	Rubrene	Organic solvent	$\sim 150 \times 10^3$ (685 nm)	0.02	0.37	Vis–vis	258
$Os(tpyCOOH)_2^{2+}$ incorporated in annihilator MOF	Zr-based CPAEBA-MOF	Solid state	$\sim 10 \times 10^3$ (724 nm)	6×10^{-5}*	0.58	Nir–vis	259
$Os(phen)_3$-DPA dyad	9-phenyl-10-(p-tolyl)anthracene	Organic solvent	132 (663 nm)	0.05*	1.12	Vis–vis	260
$Os(phen)_3^{2+}$-Pe	BPEA	Organic solvent and hydrogel	a. 86 (663 nm) b.1.4 × 10^3 (663 nm in hydrogel)	a. 0.13* b.0.04* in hydrogel	a.0.69 b.0.48 in hydrogel	Vis–vis	261
Methylene blue	DPA crystals (doped with methylene blue)	Crystals	$\sim 10^3$ (635 nm)	⋯	1.10	Vis–vis	262
4CzBN	TIPS-Naph	Organic solvent	220 (405 nm)	0.17	0.47	Vis–uv	263
4CzIPN	p-TIPS-BP	Organic solvent	$\sim 1.5 \times 10^3$ (447 nm)	0.04	1	Vis–uv	264
CBDAC	TIPS-Nph	Organic solvent	10.8 (445 nm)	0.10*	0.66	Vis–uv	265

TABLE V. (*Continued.*)

Sensitizer	Annihilator	Environment	Ith [mW cm^{-2}] (λ_{exc})	Φ_{uc}	ΔE (eV)	Spectral working range	Reference.
BN-2Cz	1,4-DTNA	Organic solvent	15.8 (517 nm)	0.04*	0.91	Vis–uv	266
BN-2Cz-tBu	1,5-DTNA	Organic solvent	29.2 (532 nm)	0.02*	1.05	Vis–uv	266

All the aforementioned upconversion processes are multiphoton mechanisms that require the simultaneous absorption of $n \geq 2$ photons or the co-existence of $n \geq 2$ excited states to enable the photophysical mechanisms resulting in the upconverted emission. This is the ultimate reason for the general dependence of ϕ_{uc} on the excitation intensity I_{exc}. The more photons the system absorbs, the larger is the probability of the multiphoton upconversion process to occur, with $\phi_{uc}(n) \propto I_{exc}^{n-1}$. Nevertheless, dealing with photoluminescent systems, we can apply to ϕ_{uc} the same definition employed for standard Stokes emitters; thus,

$$\phi_{uc} = \frac{ph_{em}}{ph_{abs}}, \tag{12}$$

where $ph_{em} = \int_{-\infty}^{+\infty} PL(\lambda)d\lambda$ is the wavelength-integrated photoluminescence spectrum $PL(\lambda)$ recorded with a photon counter and $ph_{abs} = \int_{-\infty}^{+\infty} \overline{\alpha}(\lambda)I_{exc}(\lambda)d\lambda$ is the system wavelength-integrated absorptance $\overline{\alpha}(\lambda)$ with respect to an excitation source with emission spectrum $I_{exc}(\lambda)$. By considering multiphoton upconversion mechanisms, the global yield at a fixed I_{exc} can be expressed also as

$$\phi_{uc}(n, I_{exc}) = \frac{\prod_i \phi_i}{n}, \tag{13}$$

where the index i runs over the series of involved steps, each with its own quantum efficiency ϕ_i. In the ideal case where $\prod_i \phi_i = 1$, the energy conservation law states that the maximum conversion efficiency achievable $\phi_{uc}^{\max}$ is determined by the minimum number of photons n required to activate the process. Since the TTA-UC belongs to the family of bimolecular processes, as at least $n = 2$ photons are required to create two triplets to produce a high energy singlet via TTA, it is trivial to obtain

$$\phi_{TTA-UC}^{\max} = 0.5\,[n = 2]. \tag{14}$$

Thus, for 100 photons absorbed, a maximum of 50 photons can be emitted at higher energy. Therefore, for applicative purposes, the ϕ_{uc} value measured and defined according to Eq. (12) and multiplied by the number of sub-bandgap absorbed photons represents the exact potential enhancement that a solar device able to absorb entirely the upconverted luminescence can experience.[50] For TTA-UC, in Eq. (13), the numerator is the product of the yields of sensitizers intersystem crossing (ϕ_{ISC}), net energy transfer ET (ϕ_{ET}), emitter fluorescence (ϕ_{fluo}), triplet–triplet annihilation TTA (ϕ_{TTA}), and singlet generation upon TTA ($\phi_{T\to S}$), respectively. The latter is usually constant and reported as the statistical factor f, which is determined by the fundamental electronic properties of the triplet excitons involved (see Sec. III D). For fully organic TTA upconverters, we can write

$$\begin{aligned}\phi_{uc}(I_{exc}) &= \frac{1}{n}\phi_{ISC}\phi_{ET}\phi_{fl}\phi_{T\to S}\phi_{TTA}(I_{exc}) \\ &= \frac{1}{2}f\phi_{ISC}\phi_{ET}\phi_{fl}\phi_{TTA}(I_{exc}) \quad \text{(organic)},\end{aligned} \tag{15}$$

an expression that can be adapted to the hybrid case as

$$\phi_{uc}(I_{exc}) = \frac{1}{2}f\eta\phi'_{ET}\phi''_{ET}\phi_{fl}\phi_{TTA}(I_{exc}) \quad \text{(hybrid)}. \tag{16}$$

In general, the only power-dependent factor in the productory is ϕ_{TTA}, which is directly related to the triplet density T_a, and therefore to I_{exc}, by[1,2]

$$\begin{aligned}\phi_{TTA}(I_{exc}) &= \frac{k_{TTA}}{k_{bk} + k_{T_a}^0 + k_{TTA}} = \frac{\gamma_{TT}T_a}{k_{bk} + k_{T_a}^0 + \gamma_{TT}T_a} \\ &= \frac{\gamma_{TT}\beta I_{exc}}{k_{bk} + k_{T_a}^0 + \gamma_{TT}\beta I_{exc}},\end{aligned} \tag{17}$$

where $\beta = \eta\alpha(\lambda)\phi_{ET}$ with ϕ_{ET} as the net energy transfer yield from sensitizers to the annihilator triplets [Eq. (6)]. As reported above, the parameter η takes the value of 1 in the fully organic case, while $\phi_{ET} = \phi'_{ET}\phi''_{ET}$ for hybrid materials. Equations (15) and (16) point out the dependency of the upconversion efficiency on the excitation intensity. If all the processes involved have unitary yield and ideally $f = 1$ and $\eta = 1$, both equations result in a maximum yield of 0.5, consistently with the energy conservation law, but these results can also be slightly misleading. In fact, the usual target for scientists working on photoluminescence systems is to develop materials with a maximum yield of 1 (or 100%), as the common sense would suggest. From this consideration, and probably with the aim to discuss more clearly the results obtained during the development of TTA upconverters, a modified upconversion quantum yield ($\overline{\phi}_{uc}$) definition has been introduced as

$$\overline{\phi}_{uc} = n\phi_{uc}. \tag{18}$$

Here, the conversion yield is normalized to 1 by multiplying the absolute efficiency ϕ_{uc} by the minimum number of photons required for the process. The same result can be obtained using a different definition of the TTA yield, as proposed by Zhou *et al.* to avoid the uncertainty problems related to the correct experimental evaluation of the factor f related to spin statistics.[51] In this way, the maximum efficiency achievable $\overline{\phi}_{TTA-UC}^{\max}$ is 100%, which means that all the absorbed photons participate to the upconversion, regardless of n and of the number and type of intermediate steps required. This definition has several positive aspects. It is a tool for a clear general comparison of different upconversion mechanisms, since it indicates straightforwardly the excitation condition when all absorbed photons are exploited without losses. The normalized yield value can be used to estimate the

performance of upconverters for imaging, where there are no constraints on excitation power and detection sensitivity, since one needs only anti-Stokes emitters with a reasonable efficiency to record high contrast images. Nevertheless, for some applications, it can be misleading. For example, for solar technologies applications, this definition is not appropriate, since it loses the correlation with the real life side of the experiment, i.e., the effective absolute amount of upconverted photons that can be emitted and, therefore, the effective enhancement of the electrical power production yield. It is worth pointing out that both definitions are conceptually correct and mathematically rigorous, and obviously strongly correlated despite giving different information. The controversial point is that in many cases, they are used as interchangeable quantities, without any explicit proper description, introduction, or specification. Usually, the clarifying details can be found only in the supplementary material files of published papers, thus to remove this ambiguity the authors should clearly and explicitly differentiate between upconversion quantum yield (ϕ_{uc}) and *normalized* upconversion quantum yield ($\overline{\phi}_{uc}$) in the introductory section. Finally, we would like to recall that, according to the definition derived from rate equations, the excitation threshold corresponds to the intensity at which the TTA rate equals all the other triplets decay rates. This means that half of available triplets experience TTA and can generate upconverted states, so at the threshold, the upconversion yield ϕ_{uc} is half of its maximum value achievable (both in the standard and normalized definition). Therefore, the threshold can be also directly estimated from ϕ_{uc} measurements as a function of the excitation intensity as shown in Figs. 3(b) and 3(d).

Figure 4 details the ϕ_{uc} values reported in the literature from 2005 to date. The results distribution reported points out a significant difference between the fully organic and the hybrid cases. Fully organic upconverters show a broad distribution of efficiencies, which in some cases approach the upper limit of 50%. As will be discussed in Sec. III D, this limit can be achieved employing as annihilators chromophores with specific properties that maximize the singlet generation probability upon TTA. The same chromophores can be of course coupled to inorganic light harvesters, but still none of the hybrid systems developed to date shows upconversion quantum yields even close to 20%.

C. Energy gain and spectral working range

Being a photon managing process with applicative aims, an important parameter that characterizes any upconversion process is the effective energy gain that can be achieved with respect to the excitation energy. The *s*TTA upconversion is an incoherent process so the

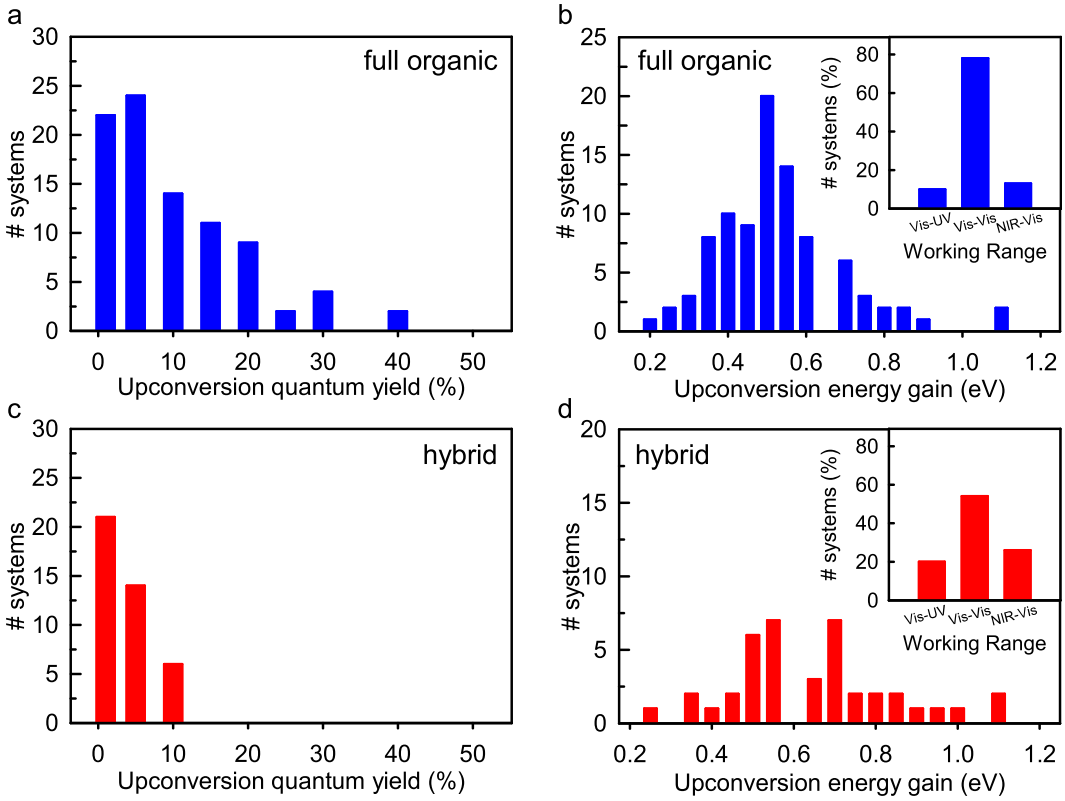

FIG. 4. Upconversion quantum yield [(a) and (b)] values and upconversion energy gain achieved [(c) and (d)] with *s*TTA upconversion in fully organic and hybrid systems from 2005 to date (see Table I). Upconversion quantum efficiency values have been grouped considering a maximum ±2% difference with respect to the reference value. The yield values are given according to the upconversion yield definition limited at 50%, so those originally expressed in the normalized form have been multiplied by a factor 0.5. The energy gain values have been grouped by considering a maximum of ±0.02 eV difference with respect to the reference value and taking into account the energy difference between the excitation wavelength and the most energetic peak in the upconverted emission spectrum.

effective energy gain is limited if compared to other coherent processes such as second harmonic generation where coherent photons are combined to generate the high-energy radiation. However, significant energetic gains have been obtained also in *s*TTA upconverting systems.

Panels (c) and (d) of Fig. 4 illustrate the energy gain distribution reported in the literature. In both fully organic and hybrid systems, a gain as large as 1.1 eV can be accomplished, while the upconverters majority show a substantial average energy gain of about 0.5–0.6 eV. However, we would like to point out that the values summarized in Fig. 4 are referred to the energy difference between the highest frequency emission peak in the upconverted emission spectrum and the frequency of the excitation light source. Therefore, the numbers reported in the literature should be treated with some care. While for fully organic systems we usually deal with narrow absorption spectra and internal energy losses to convert the excited singlets to triplets, i.e., with metallated porphyrins that are the golden standards as triplet sensitizers, in hybrid systems, the absorption band is broad and continuous. Consequently, the reported energy gain is set by the availability of excitation sources in the laboratory, while the potential gain could be larger by exciting the system in the low energy tail of the nanocrystals absorption strictly resonant with the ligand triplets. The enhanced versatility of inorganic nanocrystals as sensitizers compared to the organic counterpart is reflected also in the effective spectral working range of the systems developed to date. Among the considered papers, 77% of the upconverters based on fully organic systems work in the visible spectral range, while 10% of them can convert the absorbed visible photons to the UV spectrum and 13% from the near infrared (NIR) region to the visible one. Conversely, 54% of the reported hybrid upconverters work in the visible range, while 20% create UV radiation and a significant 26% is able to recover near infrared photons to the visible spectrum.

It is worth stressing further that as the energy gain values discussed here are not intrinsic parameters of the upconverters investigated. For the applicative aims of *s*TTA upconversion we strongly encourage the future studies to report the energy gain value calculated in a more general approach, for example, as the energy difference between the 0–0 vibronic replica (energy gap) of the organic (inorganic) light- harvester/sensitizer and the most intense emission peak of the upconverted luminescence spectrum.

D. TTA spin statistics

This particular feature of the TTA process is common in both organic and hybrid upconverters, since it is related to the annihilator's properties. We briefly describe here the major statistical factors that affect the formation of a singlet-character exciton upon the collision of two triplets. As proposed long ago, the TTA reaction can be described as illustrated in Fig. 5(a). Considering the possible combinations of the quantum-mechanical wavefunctions of the colliding triplets, the collisional complex can be described as a superposition of quintet, triplet and singlet states with relative weight of 5, 3, and 1. The branching ratio between the possible outputs is determined by several factors,[52–55] but to a first approximation, we consider the quintets as inaccessible, since they require the simultaneous excitation of two electrons. Conversely, both high-energy triplets and singlets can be accessed by combining the energy of two low-energy triplets. In the simplest case, both the T_2 and S_1 states can be populated with a statistical ratio of 3:1 [Fig. 5(b)]. However, the formed T_2 state quickly relaxes to the lowest T_1 level, so after the collision of four triplet exciton pairs five triplets are destroyed, and only two of them give a singlet, setting the statistical parameter $f = 2/5$.[5,6] On the contrary, if the $E(T_2) \gg 2E(T_1)$, the formation of high-energy triplets is prevented and only singlet excitons can be formed upon TTA, achieving the $f = 1$ [Fig. 5(c)]. This last condition is the ideal situation that allows us to bypass the statistical limits and to reach a maximum internal normalized upconversion yield of 100%.[13,56]

IV. STTA UPCONVERSION IN BIO-RELATED APPLICATIONS

In addition to solar-based technologies, upconversion is also largely studied for its application in biological systems for imaging,[57] as well as to explore unconventional *in vivo* drug photorelease[58] and other biophotonic applications.[24,59,60] Displaying the advantage of reaching high quantum yields under non-coherent low excitation intensity, in this field the *s*TTA upconversion is an excellent competing mechanism over the more classical ones that require much higher excitation intensities, potentially detrimental or fatal for the biological environment. Various systems have been realized to work in the oxygen-rich aqueous media that have to be faced in biomedical applications. Table III reports examples of micro- or nanosized upconverting particles based on TTA. Several upconverting nanoparticle-based

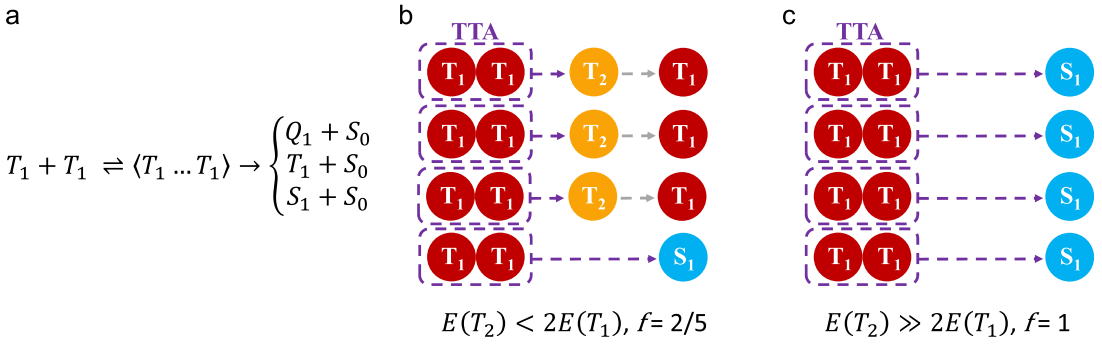

FIG. 5. (a) Sketch of the TTA process that can result in the formation of quintet, (Q), triplet (T), and singlet (S) states. If four triplet pairs are considered, in the case (b) where T_2 levels are energetically accessible, five triplets are lost to generate one singlet by exploiting only two triplets, thus the statistical factor $f = 2/5 = 0.4$. In the case (c) where the T_2 levels are energetically inaccessible, the collision of four triplet pairs produces four excited singlet states. Therefore, all triplets are exploited to generate upconverted states, $f = 8/8 = 1$ and the achievement of the maximum internal normalized upconversion yield of 100% is feasible.

approaches have been developed by using polymeric hosts, organic architectures based on a soft core with a rigid and oxygen shielding shell, as well as multicomponent crystalline nanoparticles and hollow silica hosts to embed liquid domains containing the upconverting dyes pairs. From the reported data, it is easy to see that in the "upconverting particle" architecture, good excitation thresholds of tens of mW cm^{-2} have been obtained, in some cases even orders of magnitude lower than for systems exploiting ESA in rare earth ions. Conversely, it is definitely more challenging to achieve high efficiencies, because the control of intermolecular and quenching processes is harder in quasi-solid-state confined systems. Nevertheless, it should be recalled that for these applications, the requirements of low power performance are quite relaxed with respect to solar applications, since, for example, imaging and photo-driven drug-release can be activated using laser or LED sources with the necessary power. Notably, only fully organic *s*TTA upconverters have been developed in these fields to date.

V. OVERLOOK

In this Review, we summarized the results obtained by the scientific community in the development of *s*TTA upconversion materials since the first proposals of this process as an efficient photon managing technique for non-coherent photons at low powers. Starting from its demonstration in 2006 that directly exploited the solar light, it has been deeply studied and a plethora of conjugated triplet sensitizers and annihilators pairs have been proposed, designed, and synthesized to develop efficient upconverters. These studies also revealed a variety of new applications of the *s*TTA upconversion unrelated to its initial purpose, i.e., the activation of 3D controlled polymerization and printing.[61] Several years ago, the continuous research of more versatile and more efficient upconverters moved the community from using exclusively organic conjugated species. Semiconductor nanocrystals, and more recently also perovskites, have been introduced because their finely tunable properties allow to broaden the upconversion spectral working range and to overcome the limits imposed by conjugated triplet sensitizers, which can be coupled only to specific annihilators. In general, these targets have been partially achieved. As discussed above, by employing hybrid upconverters, we can now exploit better the *s*TTA upconversion in the NIR-to-vis spectral region, with potential interesting consequences in the field of solar technologies to recover sub-bandgap photons. Conversely, the upconversion efficiency and the threshold excitation power are still lower and higher, respectively, than for the fully organic counterparts working in the same spectral range. This can be most likely ascribed to their broadband absorption, which induces more significant inner-filter losses at high concentrations, and to the complex interactions, still not fully understood, between the inorganic species and the conjugated systems that harvest the absorbed energy on their surfaces, such as the thermally activated back energy transfer. Also, optically active inorganic nanoparticles suffer from more efficient parasitic deactivation channels for excitons that are absent in conjugated molecules.

Therefore, a preferential composition to realize a *s*TTA upconverter is still missing, but the ultimate choice is primarily driven by the application. Moreover, the research is active in the development of alternative triplet sensitizers based on different mechanisms of triplet generation and manipulation, well beyond the idea to use inorganic nanoparticles as light absorbers. Table V reports a series of *s*TTA upconverters that exploit unconventional triplet sensitizers, such as thermally activated delayed fluorescence materials,[62–65] molecules with partially allowed direct S_0-T_1 absorption,[66,67] and heavy metal-free compounds.[68–71] The latter, for example, can be an elegant and efficient solution for bio-related uses, to avoid potentially toxic elements that would prevent their practical use, as already happens for common hybrid upconverters. For solar applications, the material choice is oriented toward the most efficient material that works at the lowest possible excitation, limited by the solar irradiance availability according to the features of the device to be coupled to the upconverter. However, if there is not an upper limit to the excitation power, the choice can span over a much larger sensitizer family to match the specific requirements of the application of interest. It is worth noting that several common challenges are still to be faced, regardless of the system composition.

The first is the realization of efficient upconverters in the solid state, which are much more technologically appealing. The *s*TTA upconversion is a diffusion limited bi-molecular process; thus, its effectiveness in solids is usually hindered by several factors such as poor exciton mobility, aggregation and phase segregation effects, and excited state quenching[72] that can affect the energy transfer and the TTA. Much effort has been devoted to develop solid upconverters realizing rigid nanoparticles,[46,73] nanocrystals,[74,75] polymeric films,[76,77] co-crystals,[78] and multilayer devices.[79] These architectures are indeed partially able to overcome the triplets' diffusion limits,[80–82] and particularly encouraging results have been obtained employing hybrid systems with semiconductor quantum dots[83,84] and more recently perovskites nanocrystals[29,85,86] as sensitizers. Recently, the physical confinement of the sensitizer and emitter components in colloidal nanostructures or in large molecular structures or polymeric systems, where triplet hopping between the annihilator units is allowed, has been proposed to mitigate the diffusion dependency of the TTA yield by exploiting the confined-TTA process.[87–91] In these architectures, the triplets are physically confined in discrete volumes that are smaller than the space potentially explored during diffusion; thus, if two emitter triplets are simultaneously created in such a container, they can decay only by annihilation with a forced maximized TTA yield. This mechanism enables us to reach the maximum conversion efficiency at excitation intensities lower than in classical bulks, because the triplet confinement enhances their collisional probability and also prevents the triplets from encountering quenching sites during diffusion.[74,75,87,92] Obtaining a diffusion-free intramolecular TTA mechanism would completely eliminate the problem of exciton mobility in solids. In this case, two triplets are simultaneously created on the same annihilator and can experience instantaneous TTA. The occurrence of intramolecular TTA has been hinted and demonstrated very recently,[88,93–97] opening the way to the realization of multicomponent molecular systems where both sensitizer antennas and annihilators are included in the same molecular structure to allow a complete diffusion-free upconversion process.

The second challenge regards the lack of annihilators moieties with the proper electronic structure to enable TTA and, importantly, with a *f* factor of 1. This point is crucial since it represents an intrinsic bottleneck that strongly limits the upconversion yield. To date, few examples can be found in the literature, where perylene is identified as the elected annihilator.[13,53] However, there is still great need of more efficient annihilators to cover the whole UV–Vis–NIR spectral range to expand and affirm the technological interest of the *s*TTA upconversion.

In this regard, we recently demonstrated how with a proper molecular design it is possible to obtain new annihilators that maximize the efficiency of upconverted singlets generation by TTA.[97] The quantum mechanical analysis and the spectroscopic investigation of the molecular electronic properties of the proposed chromophores suggest an unexpected energetic resonance between the low-energy T_2, which is accessible through TTA, and the emissive S_1 state. The obtained results indicate that this resonance could enable a fast delocalization of the T_2 molecular exciton on the singlet, thus avoiding the recombination of the T_2 level and the corresponding energy loss, and producing upconverted excited singlets with an efficiency that surpasses the limit imposed by classical spin-statistics in the best polyacene-based annihilators. This energetic interplay between singlet and triplet states can be, therefore, considered as a good starting point to design and produce efficient TTA annihilators involving high-energy triplets by exploiting the excellent predisposition of conjugated systems to functionalization and fine tuning of electronic properties.

To conclude, the *s*TTA upconversion mechanism has been and is still deeply studied and a huge family of materials has been developed to exploit the process in several application fields. For a general perspective, the physics of the process in fully organic systems has reached a high level of understanding, while for hybrid upconverters, there is still lack of detail about the processes occurring at the interface between the inorganic and organic phases that limit the material performances. Nevertheless, the interest dedicated to *s*TTA upconversion is continuously increasing, considering also its applicability in optoelectronic devices such as OLEDs and upconversion based solar cells. It can be exploited taking advantage of the injected charges to create the annihilating species in the former case or by harvesting the high-energy electrons from the upconverted singlets in the latter.[20,79,82,98–104] The future realization of both fully organic and hybrid systems based on optimized annihilator species will push forward the effective implementation of the *s*TTA upconversion mechanism in real life devices.

ACKNOWLEDGMENTS

The authors gratefully acknowledge the Italian Ministry of University (MUR) for financial support through Grant Dipartimenti di Eccellenza-2017 "Materials for Energy."

AUTHOR DECLARATIONS

Conflict of Interest

The authors have no conflicts to disclose.

Author Contributions

Alessandra Ronchi: Conceptualization (equal); Data curation (equal); Formal analysis (equal); Methodology (equal); Writing – original draft (equal); Writing – review & editing (equal). **Angelo Monguzzi:** Conceptualization (equal); Data curation (equal); Funding acquisition (equal); Methodology (equal); Supervision (equal); Writing – original draft (equal); Writing – review & editing (equal).

DATA AVAILABILITY

Data sharing is not applicable to this article as no new data were created or analyzed in this study.

REFERENCES

[1]J. B. Birks, *Photophysics of Aromatic Molecules* (Wiley-Interscience, London, New York, 1970).
[2]M. Pope and C. E. Swenberg, *Electronic Processes in Organic Crystals and Polymers* (Oxford University Press, New York, 1999).
[3]C. A. Parker and C. G. Hatchard, Proc. R. Soc. A **269**, 574–584 (1962).
[4]C. A. Parker and C. G. Hatchard, Trans. Faraday Soc. **59**, 284–295 (1963).
[5]R. P. Groff, R. E. Merrifield, and P. Avakian, Chem. Phys. Lett. **5**(3), 168–170 (1970).
[6]C. Murawski, K. Leo, and M. C. Gather, Adv. Mater. **25**(47), 6801–6827 (2013).
[7]P. Avakian and R. E. Merrifield, J. Phys. Rev. Lett. **13**(18), 541 (1964).
[8]J. Jortner, S.-I. Choi, J. L. Katz, and S. A. Rice, Phys. Rev. Lett. **11**(7), 323 (1963).
[9]C. K. Yong, A. J. Musser, S. L. Bayliss, S. Lukman, H. Tamura, O. Bubnova, R. K. Hallani, A. Meneau, R. Resel, M. Maruyama, S. Hotta, L. M. Herz, D. Beljonne, J. E. Anthony, J. Clark, and H. Sirringhaus, Nat. Commun. **8**(1), 15953 (2017).
[10]D. G. Bossanyi, M. Matthiesen, S. Wang, J. A. Smith, R. C. Kilbride, J. D. Shipp, D. Chekulaev, E. Holland, J. E. Anthony, J. Zaumseil, A. J. Musser, and J. Clark, Nat. Chem. **13**(2), 163–171 (2021).
[11]R. R. Islangulov, D. V. Kozlov, and F. N. Castellano, Chem. Commun. **2005**(30), 3776–3778.
[12]S. Baluschev, T. Miteva, V. Yakutkin, G. Nelles, A. Yasuda, and G. Wegner, Phys. Rev. Lett. **97**(14), 143903 (2006).
[13]W. Sun, A. Ronchi, T. Zhao, J. Han, A. Monguzzi, and P. Duan, J. Mater. Chem. C **9**(40), 14201–14208 (2021).
[14]C. Strümpel, M. McCann, G. Beaucarne, V. Arkhipov, A. Slaoui, V. Švrček, C. D. Cañizo, and I. Tobias, Sol. Energy Mater. Sol. Cells **91**(4), 238–249 (2007).
[15]G. Chen, C. Yang, and P. N. Prasad, Acc. Chem. Res. **46**(7), 1474–1486 (2013).
[16]F. Auzel, Chem. Rev. **104**(1), 139–174 (2004).
[17]M. Pawlicki, H. A. Collins, R. G. Denning, and H. L. Anderson, Angew. Chem. Int. Ed. **48**(18), 3244–3266 (2009).
[18]J. Zhou, Z. Liu, and F. Li, Chem. Soc. Rev. **41**(3), 1323–1349 (2012).
[19]H.-I. Kim, O. S. Kwon, S. Kim, W. Choi, and J.-H. Kim, Energy Environ. Sci. **9**(3), 1063–1073 (2016).
[20]S. P. Hill and K. Hanson, J. Am. Chem. Soc. **139**(32), 10988–10991 (2017).
[21]J. Pedrini and A. Monguzzi, J. Photonics Energy **8**(2), 022005 (2017).
[22]T. F. Schulze and T. W. Schmidt, Energy Environ. Sci. **8**(1), 103–125 (2015).
[23]Q. Liu, M. Xu, T. Yang, B. Tian, X. Zhang, and F. Li, ACS Appl. Mater. Interfaces **10**(12), 9883–9888 (2018).
[24]J. Park, M. Xu, F. Li, and H.-C. Zhou, J. Am. Chem. Soc. **140**(16), 5493–5499 (2018).
[25]Y. Sasaki, M. Oshikawa, P. Bharmoria, H. Kouno, A. Hayashi-Takagi, M. Sato, I. Ajioka, N. Yanai, and N. Kimizuka, Angew. Chem. **131**(49), 17991–17997 (2019).
[26]A. L. Hagstrom, H.-L. Lee, M.-S. Lee, H.-S. Choe, J. Jung, B.-G. Park, W.-S. Han, J.-S. Ko, J.-H. Kim, and J.-H. Kim, ACS Appl. Mater. Interfaces **10**(10), 8985–8992 (2018).
[27]L. Huang, T. Le, K. Huang, and G. Han, Nat. Commun. **12**(1), 1898 (2021).
[28]C. Mongin, S. Garakyaraghi, N. Razgoniaeva, M. Zamkov, and N. C. Felix, Science **351**(6271), 369–372 (2016).
[29]L. Nienhaus, J.-P. Correa-Baena, S. Wieghold, M. Einzinger, T.-A. Lin, K. E. Shulenberger, N. D. Klein, M. Wu, V. Bulovic, T. Buonassisi *et al.*, ACS Energy Lett. **4**(4), 888–895 (2019).
[30]Z. Huang, Z. Xu, M. Mahboub, Z. Liang, P. Jaimes, P. Xia, K. R. Graham, M. L. Tang, and T. Lian, J. Am. Chem. Soc. **141**(25), 9769–9772 (2019).
[31]C. J. Imperiale, P. B. Green, M. Hasham, and M. W. B. Wilson, Chem. Sci. **12**(42), 14111–14120 (2021).
[32]D. Thomas David, F. Carlsen William, and L. Stryer, Proc. Natl. Acad. Sci. **75**(12), 5746–5750 (1978).
[33]A. Ronchi and A. Monguzzi, J. Appl. Phys. **129**(5), 050901 (2021).
[34]A. Monguzzi, R. Tubino, M. M. Salamone, and F. Meinardi, Phys. Rev. B **82**(12), 125113 (2010).
[35]A. Monguzzi, J. Mezyk, F. Scotognella, R. Tubino, and F. Meinardi, Phys. Rev. B **78**(19), 195112 (2008).

[36]L. Frazer, J. K. Gallaher, and T. W. Schmidt, ACS Energy Lett. **2**(6), 1346–1354 (2017).
[37]D. Meroni, A. Monguzzi, and F. Meinardi, J. Chem. Phys. **153**(11), 114302 (2020).
[38]A. Monguzzi, R. Tubino, S. Hoseinkhani, M. Campione, and F. Meinardi, Phys. Chem. Chem. Phys. **14**(13), 4322–4332 (2012).
[39]M. Montalti *et al.*, *Handbook of Photochemistry* (CRC Press, 2020).
[40]T. X. Ding, J. H. Olshansky, S. R. Leone, and A. P. Alivisatos, J. Am. Chem. Soc. **137**(5), 2021–2029 (2015).
[41]A. Ronchi, C. Capitani, V. Pinchetti, G. Gariano, M. L. Zaffalon, F. Meinardi, S. Brovelli, and A. Monguzzi, Adv. Mater. **32**(37), 2002953 (2020).
[42]Y. Han, S. He, X. Luo, Y. Li, Z. Chen, W. Kang, X. Wang, and K. Wu, J. Am. Chem. Soc. **141**(33), 13033–13037 (2019).
[43]X. Luo, Y. Han, Z. Chen, Y. Li, G. Liang, X. Liu, T. Ding, C. Nie, M. Wang, F. N. Castellano, and K. Wu, Nat. Commun. **11**(1), 28 (2020).
[44]Z. Xu, Z. Huang, T. Jin, T. Lian, and M. L. Tang, Acc. Chem. Res. **54**(1), 70–80 (2021).
[45]P. B. Green, F. Yarur Villanueva, C. J. Imperiale, M. Hasham, K. Z. Demmans, D. C. Burns, and M. W. B. Wilson, ACS Appl. Nano Mater. **4**(6), 5655–5664 (2021).
[46]J. Perego, J. Pedrini, C. X. Bezuidenhout, P. E. Sozzani, F. Meinardi, S. Bracco, A. Comotti, and A. Monguzzi, Adv. Mater. **31**(40), 1903309 (2019).
[47]Y. Murakami and K. Kamada, Phys. Chem. Chem. Phys. **23**(34), 18268–18282 (2021).
[48]A. Monguzzi, D. Braga, M. Gandini, V. Holmberg, D. K. Kim, A. Sahu, D. J. Norris, and F. Meinardi, Nano Lett. **14**(11), 6644–6650 (2014).
[49]F. Edhborg, A. Olesund, and B. Albinsson, Photochem. Photobiol. Sci. **21**, 1143–1158 (2022).
[50]N. Yanai, K. Suzuki, T. Ogawa, Y. Sasaki, N. Harada, and N. Kimizuka, J. Phys. Chem. A **123**(46), 10197–10203 (2019).
[51]Y. Zhou, F. N. Castellano, T. W. Schmidt, and K. Hanson, ACS Energy Lett. **5**(7), 2322–2326 (2020).
[52]J. Mezyk, R. Tubino, A. Monguzzi, A. Mech, and F. Meinardi, Phys. Rev. Lett. **102**(8), 087404 (2009).
[53]Y. Y. Cheng, B. Fückel, T. Khoury, R. G. Clady, M. J. Tayebjee, N. Ekins-Daukes, M. J. Crossley, and T. W. Schmidt, J. Phys. Chem. Lett. **1**(12), 1795–1799 (2010).
[54]Y. Y. Cheng, T. Khoury, R. G. Clady, M. J. Tayebjee, N. Ekins-Daukes, M. J. Crossley, and T. W. Schmidt, Phys. Chem. Chem. Phys. **12**(1), 66–71 (2010).
[55]D. G. Bossanyi, Y. Sasaki, S. Wang, D. Chekulaev, N. Kimizuka, N. Yanai, and J. Clark, JACS Au **1**(12), 2188–2201 (2021).
[56]S. Hoseinkhani, R. Tubino, F. Meinardi, and A. Monguzzi, Phys. Chem. Chem. Phys. **17**(6), 4020–4024 (2015).
[57]F. Wang, D. Banerjee, Y. Liu, X. Chen, and X. Liu, Analyst **135**(8), 1839–1854 (2010).
[58]M. Peña-López and M. Beller, Angew. Chem. Int. Ed. **56**(1), 46–48 (2017).
[59]S. H. Askes, N. L. Mora, R. Harkes, R. I. Koning, B. Koster, T. Schmidt, A. Kros, and S. Bonnet, Chem. Commun. **51**(44), 9137–9140 (2015).
[60]S. H. Askes, W. Pomp, S. L. Hopkins, A. Kros, S. Wu, T. Schmidt, and S. Bonnet, Small **12**(40), 5579–5590 (2016).
[61]Z. Wang, Y. Hou, Z. Huo, Q. Liu, W. Xu, and J. Zhao, Chem. Commun. **57**(72), 9044–9047 (2021).
[62]T. C. Wu, D. N. Congreve, and M. A. Baldo, Appl. Phys. Lett. **107**(3), 031103 (2015).
[63]N. Yanai, M. Kozue, S. Amemori, R. Kabe, C. Adachi, and N. Kimizuka, J. Mater. Chem. C **4**(27), 6447–6451 (2016).
[64]D. Wei, F. Ni, Z. Zhu, Y. Zou, and C. Yang, J. Mater. Chem. C **5**(48), 12674–12677 (2017).
[65]W. Chen, F. Song, S. Tang, G. Hong, Y. Wu, and X. Peng, Chem. Commun. **55**(30), 4375–4378 (2019).
[66]S. Amemori, Y. Sasaki, N. Yanai, and N. Kimizuka, J. Am. Chem. Soc. **138**(28), 8702–8705 (2016).
[67]Y. Wei, M. Zheng, L. Chen, X. Zhou, and S. Liu, Dalton Trans. **48**(31), 11763–11771 (2019).
[68]W. Wu, J. Zhao, J. Sun, and S. Guo, J. Org. Chem. **77**(12), 5305–5312 (2012).
[69]D. Huang, J. Sun, L. Ma, C. Zhang, and J. Zhao, Photochem. Photobiol. Sci. **12**(5), 872–882 (2013).
[70]Y. Wei, M. Zhou, Q. Zhou, X. Zhou, S. Liu, S. Zhang, and B. Zhang, Phys. Chem. Chem. Phys. **19**(33), 22049–22060 (2017).
[71]Q. Chen, Y. Liu, X. Guo, J. Peng, S. Garakyaraghi, C. M. Papa, F. N. Castellano, D. Zhao, and Y. Ma, J. Phys. Chem. A **122**(33), 6673–6682 (2018).
[72]Y. Deng, L. Jiang, L. Huang, and T. Zhu, ACS Energy Lett. **7**(2), 847–861 (2022).
[73]W. Wang, Q. Liu, C. Zhan, A. Barhoumi, T. Yang, R. G. Wylie, P. A. Armstrong, and D. S. Kohane, Nano Lett. **15**(10), 6332–6338 (2015).
[74]F. Meinardi, M. Ballabio, N. Yanai, N. Kimizuka, A. Bianchi, M. Mauri, R. Simonutti, A. Ronchi, M. Campione, and A. Monguzzi, Nano Lett. **19**(3), 2169–2177 (2019).
[75]I. Roy, S. Goswami, R. M. Young, I. Schlesinger, M. R. Mian, A. E. Enciso, X. Zhang, J. E. Hornick, O. K. Farha, M. R. Wasielewski, J. T. Hupp, and J. F. Stoddart, J. Am. Chem. Soc. **143**(13), 5053–5059 (2021).
[76]Y. C. Simon and C. Weder, J. Mater. Chem. **22**(39), 20817–20830 (2012).
[77]J. Peng, X. Guo, X. Jiang, D. Zhao, and Y. Ma, Chem. Sci. **7**(2), 1233–1237 (2016).
[78]K. Kamada, Y. Sakagami, T. Mizokuro, Y. Fujiwara, K. Kobayashi, K. Narushima, S. Hirata, and M. Vacha, Mater. Horiz. **4**(1), 83–87 (2017).
[79]K. M. Felter, M. C. Fravventura, E. Koster, R. D. Abellon, T. J. Savenije, and F. C. Grozema, ACS Energy Lett. **5**(1), 124–129 (2020).
[80]S. P. Hill, T. Dilbeck, E. Baduell, and K. Hanson, ACS Energy Lett. **1**(1), 3–8 (2016).
[81]M. Oldenburg, A. Turshatov, D. Busko, S. Wollgarten, M. Adams, N. Baroni, A. Welle, E. Redel, C. Wöll, B. S. Richards, and I. A. Howard, Adv. Mater. **28**(38), 8477–8482 (2016).
[82]S. Izawa and M. Hiramoto, Nat. Photonics **15**(12), 895–900 (2021).
[83]M. Wu, D. N. Congreve, M. W. Wilson, J. Jean, N. Geva, M. Welborn, T. Van Voorhis, V. Bulović, M. G. Bawendi, and M. A. Baldo, Nat. Photonics **10**(1), 31–34 (2016).
[84]M. Wu, T.-A. Lin, J. O. Tiepelt, V. Bulović, and M. A. Baldo, Nano Lett. **21**(2), 1011–1016 (2021).
[85]M. Koharagi, N. Harada, K. Okumura, J. Miyano, S. Hisamitsu, N. Kimizuka, and N. Yanai, Nanoscale **13**, 19890–19893 (2021).
[86]Z. A. Van Orman and L. Nienhaus, ACS Energy Lett. **6**(10), 3686–3694 (2021).
[87]F. Saenz, A. Ronchi, M. Mauri, R. Vadrucci, F. Meinardi, A. Monguzzi, and C. Weder, Adv. Funct. Mater. **31**(1), 2004495 (2021).
[88]D. Dzebo, K. Börjesson, V. Gray, K. Moth-Poulsen, and B. Albinsson, J. Phys. Chem. C **120**(41), 23397–23406 (2016).
[89]F. Edhborg, H. Bildirir, P. Bharmoria, K. Moth-Poulsen, and B. Albinsson, J. Phys. Chem. B **125**(23), 6255–6263 (2021).
[90]A. J. Tilley, B. E. Robotham, R. P. Steer, and K. P. Ghiggino, Chem. Phys. Lett. **618**, 198–202 (2015).
[91]M. Sittig, B. Schmidt, H. Görls, T. Bocklitz, M. Wächtler, S. Zechel, M. D. Hager, and B. Dietzek, Phys. Chem. Chem. Phys. **22**(7), 4072–4079 (2020).
[92]F. Saenz, A. Ronchi, M. Mauri, D. Kiebala, A. Monguzzi, and C. Weder, ACS Appl. Mater. Interfaces **13**(36), 43314–43322 (2021).
[93]A. Olesund, V. Gray, J. Mårtensson, and B. Albinsson, J. Am. Chem. Soc. **143**(15), 5745–5754 (2021).
[94]A. B. Pun, S. N. Sanders, M. Y. Sfeir, L. M. Campos, and D. N. Congreve, Chem. Sci. **10**(14), 3969–3975 (2019).
[95]C. Gao, S. K. Prasad, B. Zhang, M. Dvořák, M. J. Tayebjee, D. R. McCamey, T. W. Schmidt, T. A. Smith, and W. W. H. Wong, J. Phys. Chem. C **123**(33), 20181–20187 (2019).
[96]C. J. Imperiale, P. B. Green, E. G. Miller, N. H. Damrauer, and M. W. B. Wilson, J. Phys. Chem. Lett. **10**(23), 7463–7469 (2019).
[97]S. Mattiello, S. Mecca, A. Ronchi, A. Calascibetta, G. Mattioli, F. Pallini, F. Meinardi, L. Beverina, and A. Monguzzi, ACS Energy Lett. **7**, 2435–2442 (2022).
[98]T. Dilbeck, S. P. Hill, and K. Hanson, J. Mater. Chem. A **5**(23), 11652–11660 (2017).
[99]D. Beery, T. W. Schmidt, and K. Hanson, ACS Appl. Mater. Interfaces **13**(28), 32601–32605 (2021).
[100]S. Izawa, M. Morimoto, S. Naka, and M. Hiramoto, Adv. Opt. Mater. **10**(4), 2101710 (2022).

[101]N. A. Kukhta, T. Matulaitis, D. Volyniuk, K. Ivaniuk, P. Turyk, P. Stakhira, J. V. Grazulevicius, and A. P. Monkman, J. Phys. Chem. Lett. **8**(24), 6199–6205 (2017).
[102]D. Di, L. Yang, J. M. Richter, L. Meraldi, R. M. Altamimi, A. Y. Alyamani, D. Credgington, K. P. Musselman, J. L. MacManus-Driscoll, and R. H. Friend, Adv. Mater. **29**(13), 1605987 (2017).
[103]A. Shukla, M. Hasan, G. Banappanavar, V. Ahmad, J. Sobus, E. G. Moore, D. Kabra, S.-C. Lo, and E. B. Namdas, Commun. Mater. **3**(1), 27 (2022).
[104]S.-Y. Hwang, D. Song, E.-J. Seo, F. Hollmann, Y. You, and J.-B. Park, Sci. Rep. **12**(1), 9397 (2022).
[105]W. Zhao and F. N. Castellano, J. Phys. Chem. A **110**(40), 11440–11445 (2006).
[106]S. Baluschev, V. Yakutkin, T. Miteva, Y. Avlasevich, S. Chernov, S. Aleshchenkov, G. Nelles, A. Cheprakov, A. Yasuda, K. Müllen, and G. Wegner, Angew. Chem. Int. Ed. **46**(40), 7693–7696 (2007).
[107]S. Baluschev, V. Yakutkin, G. Wegner, T. Miteva, G. Nelles, A. Yasuda, S. Chernov, S. Aleshchenkov, and A. Cheprakov, Appl. Phys. Lett. **90**(18), 181103 (2007).
[108]V. Yakutkin, S. Aleshchenkov, S. Chernov, T. Miteva, G. Nelles, A. Cheprakov, and S. Baluschev, Chem. Eur. J. **14**(32), 9846–9850 (2008).
[109]T. N. Singh-Rachford and F. N. Castellano, J. Phys. Chem. A **112**(16), 3550–3556 (2008).
[110]S. Baluschev, V. Yakutkin, T. Miteva, G. Wegner, T. Roberts, G. Nelles, A. Yasuda, S. Chernov, S. Aleshchenkov, and A. Cheprakov, New J. Phys. **10**(1), 013007 (2008).
[111]T. N. Singh-Rachford, A. Haefele, R. Ziessel, and F. N. Castellano, J. Am. Chem. Soc. **130**(48), 16164–16165 (2008).
[112]T. N. Singh-Rachford and F. N. Castellano, Inorg. Chem. **48**(6), 2541–2548 (2009).
[113]S. K. Sugunan, U. Tripathy, S. M. K. Brunet, M. F. Paige, and R. P. Steer, J. Phys. Chem. A **113**(30), 8548–8556 (2009).
[114]T. N. Singh-Rachford and F. N. Castellano, J. Phys. Chem. Lett. **1**(1), 195–200 (2010).
[115]T. N. Singh-Rachford, A. Nayak, M. L. Muro-Small, S. Goeb, M. J. Therien, and F. N. Castellano, J. Am. Chem. Soc. **132**(40), 14203–14211 (2010).
[116]K. Tanaka, K. Inafuku, and Y. Chujo, Chem. Commun. **46**(24), 4378–4380 (2010).
[117]S. Ji, W. Wu, W. Wu, H. Guo, and J. Zhao, Angew. Chem. Int. Ed. **50**(7), 1626–1629 (2011).
[118]R. S. Khnayzer, J. Blumhoff, J. A. Harrington, A. Haefele, F. Deng, and F. N. Castellano, Chem. Commun. **48**(2), 209–211 (2012).
[119]J.-H. Kim, F. Deng, F. N. Castellano, and J.-H. Kim, Chem. Mater. **24**(12), 2250–2252 (2012).
[120]A. Monguzzi, M. Frigoli, C. Larpent, R. Tubino, and F. Meinardi, Adv. Funct. Mater. **22**(1), 139–143 (2012).
[121]Y. Chen, J. Zhao, L. Xie, H. Guo, and Q. Li, RSC Adv. **2**(9), 3942–3953 (2012).
[122]S. Guo, W. Wu, H. Guo, and J. Zhao, J. Org. Chem. **77**(8), 3933–3943 (2012).
[123]J.-H. Kang and E. Reichmanis, Angew. Chem. Int. Ed. **51**(47), 11841–11844 (2012).
[124]F. Deng, J. R. Sommer, M. Myahkostupov, K. S. Schanze, and F. N. Castellano, Chem. Commun. **49**(67), 7406–7408 (2013).
[125]X. Yi, P. Yang, D. Huang, and J. Zhao, Dyes Pigm. **96**(1), 104–115 (2013).
[126]P. Duan, N. Yanai, and N. Kimizuka, J. Am. Chem. Soc. **135**(51), 19056–19059 (2013).
[127]C. Wohnhaas, K. Friedemann, D. Busko, K. Landfester, S. Baluschev, D. Crespy, and A. Turshatov, ACS Macro Lett. **2**(5), 446–450 (2013).
[128]A. Monguzzi, F. Bianchi, A. Bianchi, M. Mauri, R. Simonutti, R. Ruffo, R. Tubino, and F. Meinardi, Adv. Energy Mater. **3**(5), 680–686 (2013).
[129]Z. Jiang, M. Xu, F. Li, and Y. Yu, J. Am. Chem. Soc. **135**(44), 16446–16453 (2013).
[130]X. Cui, J. Zhao, P. Yang, and J. Sun, Chem. Commun. **49**(87), 10221–10223 (2013).
[131]W.-P. To, K. T. Chan, G. S. M. Tong, C. Ma, W.-M. Kwok, X. Guan, K.-H. Low, and C.-M. Che, Angew. Chem. Int. Ed. **52**(26), 6648–6652 (2013).
[132]P. Duan, N. Yanai, and N. Kimizuka, Chem. Commun. **50**(86), 13111–13113 (2014).
[133]F. Deng, W. Sun, and F. N. Castellano, Photochem. Photobiol. Sci. **13**(5), 813–819 (2014).
[134]B. Wang, B. Sun, X. Wang, C. Ye, P. Ding, Z. Liang, Z. Chen, X. Tao, and L. Wu, J. Phys. Chem. C **118**(3), 1417–1425 (2014).
[135]J.-H. Kim, F. Deng, F. N. Castellano, and J.-H. Kim, ACS Photonics **1**(4), 382–388 (2014).
[136]J. Peng, X. Jiang, X. Guo, D. Zhao, and Y. Ma, Chem. Commun. **50**(58), 7828–7830 (2014).
[137]S. H. Lee, M. A. Ayer, R. Vadrucci, C. Weder, and Y. C. Simon, Polym. Chem. **5**(24), 6898–6904 (2014).
[138]A. J. Svagan, D. Busko, Y. Avlasevich, G. Glasser, S. Baluschev, and K. Landfester, ACS Nano **8**(8), 8198–8207 (2014).
[139]S. Amemori, N. Yanai, and N. Kimizuka, Phys. Chem. Chem. Phys. **17**(35), 22557–22560 (2015).
[140]A. Monguzzi, S. M. Borisov, J. Pedrini, I. Klimant, M. Salvalaggio, P. Biagini, F. Melchiorre, C. Lelii, and F. Meinardi, Adv. Funct. Mater. **25**(35), 5617–5624 (2015).
[141]C. E. McCusker and F. N. Castellano, Inorg. Chem. **54**(12), 6035–6042 (2015).
[142]X. Yu, X. Cao, X. Chen, N. Ayres, and P. Zhang, Chem. Commun. **51**(3), 588–591 (2015).
[143]S. Yu, Y. Zeng, J. Chen, T. Yu, X. Zhang, G. Yang, and Y. Li, RSC Adv. **5**(86), 70640–70648 (2015).
[144]T. Ogawa, N. Yanai, A. Monguzzi, and N. Kimizuka, Sci. Rep. **5**(1), 10882 (2015).
[145]S. Hisamitsu, N. Yanai, and N. Kimizuka, Angew. Chem. Int. Ed. **54**(39), 11550–11554 (2015).
[146]P. Duan, N. Yanai, H. Nagatomi, and N. Kimizuka, J. Am. Chem. Soc. **137**(5), 1887–1894 (2015).
[147]R. Vadrucci, C. Weder, and Y. C. Simon, Mater. Horiz. **2**(1), 120–124 (2015).
[148]H. Kouno, T. Ogawa, S. Amemori, P. Mahato, N. Yanai, and N. Kimizuka, Chem. Sci. **7**(8), 5224–5229 (2016).
[149]P. Mahato, A. Monguzzi, N. Yanai, T. Yamada, and N. Kimizuka, Nat. Mater. **14**(9), 924–930 (2015).
[150]A. Monguzzi, M. Mauri, A. Bianchi, M. K. Dibbanti, R. Simonutti, and F. Meinardi, J. Phys. Chem. C **120**(5), 2609–2614 (2016).
[151]J. L. Han, J. You, H. Yonemura, S. Yamada, S. R. Wang, and X. G. Li, Photochem. Photobiol. Sci. **15**(8), 1039–1045 (2016).
[152]Y. Lu, J. Wang, N. McGoldrick, X. Cui, J. Zhao, C. Caverly, B. Twamley, G. M. Ó Máille, B. Irwin, R. Conway-Kenny, and S. M. Draper, Angew. Chem. Int. Ed. **55**(47), 14688–14692 (2016).
[153]C. Mongin, J. H. Golden, and F. N. Castellano, ACS Appl. Mater. Interfaces **8**(36), 24038–24048 (2016).
[154]V. Gray, K. Börjesson, D. Dzebo, M. Abrahamsson, B. Albinsson, and K. Moth-Poulsen, J. Phys. Chem. C **120**(34), 19018–19026 (2016).
[155]Y. Murakami, Y. Himuro, T. Ito, R. Morita, K. Niimi, and N. Kiyoyanagi, J. Phys. Chem. B **120**(4), 748–755 (2016).
[156]D. C. Thévenaz, S. H. Lee, F. Guignard, S. Balog, M. Lattuada, C. Weder, and Y. C. Simon, Macromol. Rapid Commun. **37**(10), 826–832 (2016).
[157]K. A. El Roz and F. N. Castellano, Chem. Commun. **53**(85), 11705–11708 (2017).
[158]J.-H. Kang, S. S. Lee, J. Guerrero, A. Fernandez-Nieves, S.-H. Kim, and E. Reichmanis, Adv. Mater. **29**(21), 1606830 (2017).
[159]A. L. Hagstrom, F. Deng, and J.-H. Kim, ACS Photonics **4**(1), 127–137 (2017).
[160]A. Monguzzi, A. Oertel, D. Braga, A. Riedinger, D. K. Kim, P. N. Knüsel, A. Bianchi, M. Mauri, R. Simonutti, D. J. Norris, and F. Meinardi, ACS Appl. Mater. Interfaces **9**(46), 40180–40186 (2017).
[161]J. Han, F. Zhang, J. You, Y. Hiroaki, S. Yamada, T. Morifuji, S. Wang, and X. Li, Photochem. Photobiol. Sci. **16**(9), 1384–1390 (2017).
[162]C. Ye, J. Ma, S. Chen, J. Ge, W. Yang, Q. Zheng, X. Wang, Z. Liang, and Y. Zhou, J. Phys. Chem. C **121**(37), 20158–20164 (2017).
[163]S. Chandrasekaran, Y.-L. T. Ngo, L. Sui, E. J. Kim, D. K. Dang, J. S. Chung, and S. H. Hur, Dalton Trans. **46**(40), 13912–13919 (2017).
[164]P. Bharmoria, S. Hisamitsu, H. Nagatomi, T. Ogawa, M.-A. Morikawa, N. Yanai, and N. Kimizuka, J. Am. Chem. Soc. **140**(34), 10848–10855 (2018).
[165]N. A. Durandin, J. Isokuortti, A. Efimov, E. Vuorimaa-Laukkanen, N. V. Tkachenko, and T. Laaksonen, Chem. Commun. **54**(99), 14029–14032 (2018).

[166]C. Fan, L. Wei, T. Niu, M. Rao, G. Cheng, J. J. Chruma, W. Wu, and C. Yang, J. Am. Chem. Soc. **141**(38), 15070–15077 (2019).
[167]A. B. Pun, L. M. Campos, and D. N. Congreve, J. Am. Chem. Soc. **141**(9), 3777–3781 (2019).
[168]J. Ma, S. Chen, C. Ye, M. Li, T. Liu, X. Wang, and Y. Song, Phys. Chem. Chem. Phys. **21**(27), 14516–14520 (2019).
[169]A. Abulikemu, Y. Sakagami, C. Heck, K. Kamada, H. Sotome, H. Miyasaka, D. Kuzuhara, and H. Yamada, ACS Appl. Mater. Interfaces **11**(23), 20812–20819 (2019).
[170]M. Kinoshita, Y. Sasaki, S. Amemori, N. Harada, Z. Hu, Z. Liu, L. K. Ono, Y. Qi, N. Yanai, and N. Kimizuka, ChemPhotoChem **4**(11), 5271–5278 (2020).
[171]L. Huang, W. Wu, Y. Li, K. Huang, L. Zeng, W. Lin, and G. Han, J. Am. Chem. Soc. **142**(43), 18460–18470 (2020).
[172]X. Yu, C. Fan, G. Dai, X. Wang, C. Ye, and X. Tao, Dyes Pigm. **176**, 108166 (2020).
[173]R. Fayad, A. T. Bui, S. G. Shepard, and F. N. Castellano, ACS Appl. Energy Mater. **3**(12), 12557–12564 (2020).
[174]E. Radiunas, S. Raišys, S. Juršėnas, A. Jozeliūnaitė, T. Javorskis, U. Šinkevičiūtė, E. Orentas, and K. Kazlauskas, J. Mater. Chem. C 8, 5525–5534 (2020).
[175]Z. Mahmood, N. Rehmat, S. Ji, J. Zhao, S. Sun, M. D. Donato, M. Li, M. Teddei, and Y. Huo, Chem. Eur. J. **26**(65), 14912–14918 (2020).
[176]B. Pfund, D. M. Steffen, M. R. Schreier, M.-S. Bertrams, C. Ye, K. Börjesson, O. S. Wenger, and C. Kerzig, J. Am. Chem. Soc. **142**(23), 10468–10476 (2020).
[177]S. Hisamitsu, J. Miyano, K. Okumura, J. K.-H. Hui, N. Yanai, and N. Kimizuka, ChemistryOpen **9**(1), 14–17 (2020).
[178]Z.-Y. Zou, Ping-Ding, X.-M. Wang, Z.-Q. Liang, and X.-T. Tao, ChemistrySelect **5**(5), 1713–1717 (2020).
[179]M. Yang, S. Sheykhi, Y. Zhang, C. Milsmann, and F. N. Castellano, Chem. Sci. **12**(26), 9069–9077 (2021).
[180]J. S. Lissau, M. Khelfallah, and M. Madsen, J. Phys. Chem. C **125**(46), 25643–25650 (2021).
[181]N. Harada, Y. Sasaki, M. Hosoyamada, N. Kimizuka, and N. Yanai, Angew. Chem. Int. Ed. **60**(1), 142–147 (2021).
[182]W. Sun, A. Ronchi, T. Zhao, J. Han, A. Monguzzi, and P. Duan, J. Mater. Chem. C **9**, 14201–14208 (2021).
[183]J. B. Bilger, C. Kerzig, C. B. Larsen, and O. S. Wenger, J. Am. Chem. Soc. **143**(3), 1651–1663 (2021).
[184]P. Bharmoria, S. Hisamitsu, Y. Sasaki, T. S. Kang, M.-A. Morikawa, B. Joarder, K. Moth-Poulsen, H. Bildirir, A. Mårtensson, N. Yanai, and N. Kimizuka, J. Mater. Chem. C **9**(35), 11655–11661 (2021).
[185]Y. J. Yun, J. Isokuortti, T. Laaksonen, N. Durandin, and A. J.-L. Ayitou, J. Photochem. Photobiol. A: Chem. **418**, 113412 (2021).
[186]L. Yang, X. W. Chua, Z. Yang, X. Ding, Y. Yu, A. Suwardi, M. Zhao, K. L. Ke, B. Ehrler, and D. Di, Nanoscale Adv. **4**(5), 1318–1323 (2022).
[187]Y. Y. Cheng, B. Fückel, T. Khoury, R. G. C. R. Clady, N. J. Ekins-Daukes, M. J. Crossley, and T. W. Schmidt, J. Phys. Chem. A **115**(6), 1047–1053 (2011).
[188]Z. Huang, X. Li, M. Mahboub, K. M. Hanson, V. M. Nichols, H. Le, M. L. Tang, and C. J. Bardeen, Nano Lett. **15**(8), 5552–5557 (2015).
[189]Z. Huang, X. Li, B. D. Yip, J. M. Rubalcava, C. J. Bardeen, and M. L. Tang, Chem. Mater. **27**(21), 7503–7507 (2015).
[190]K. Okumura, K. Mase, N. Yanai, and N. Kimizuka, Chem. Eur. J. **22**(23), 7721–7726 (2016).
[191]Z. Huang, D. E. Simpson, M. Mahboub, X. Li, and M. L. Tang, Chem. Sci. **7**(7), 4101–4104 (2016).
[192]M. Mahboub, Z. Huang, and M. L. Tang, Nano Lett. **16**(11), 7169–7175 (2016).
[193]X. Li, Z. Huang, R. Zavala, and M. L. Tang, J. Phys. Chem. Lett. **7**(11), 1955–1959 (2016).
[194]V. Gray, P. Xia, Z. Huang, E. Moses, A. Fast, D. A. Fishman, V. I. Vullev, M. Abrahamsson, K. Moth-Poulsen, and M. L. Tang, Chem. Sci. **8**(8), 5488–5496 (2017).
[195]L. Nienhaus, M. Wu, N. Geva, J. J. Shepherd, M. W. B. Wilson, V. Bulović, T. Van Voorhis, M. A. Baldo, and M. G. Bawendi, ACS Nano **11**(8), 7848–7857 (2017).
[196]K. Mase, K. Okumura, N. Yanai, and N. Kimizuka, Chem. Commun. **53**(59), 8261–8264 (2017).
[197]Z. Huang, P. Xia, N. Megerdich, D. A. Fishman, V. I. Vullev, and M. L. Tang, ACS Photonics **5**(8), 3089–3096 (2018).
[198]S. Amemori, R. K. Gupta, M. L. Böhm, J. Xiao, U. Huynh, T. Oyama, K. Kaneko, A. Rao, N. Yanai, and N. Kimizuka, Dalton Trans. **47**(26), 8590–8594 (2018).
[199]S. He, X. Luo, X. Liu, Y. Li, and K. Wu, J. Phys. Chem. Lett. **10**(17), 5036–5040 (2019).
[200]K. Okumura, N. Yanai, and N. Kimizuka, Chem. Lett. **48**(11), 1347–1350 (2019).
[201]A. Ronchi, P. Brazzo, M. Sassi, L. Beverina, J. Pedrini, F. Meinardi, and A. Monguzzi, Phys. Chem. Chem. Phys. **21**(23), 12353–12359 (2019).
[202]N. Nishimura, J. R. Allardice, J. Xiao, Q. Gu, V. Gray, and A. Rao, Chem. Sci. **10**(18), 4750–4760 (2019).
[203]Z. A. VanOrman, A. S. Bieber, S. Wieghold, and L. Nienhaus, Chem. Mater. **32**(11), 4734–4742 (2020).
[204]P. Xia, E. K. Raulerson, D. Coleman, C. S. Gerke, L. Mangolini, M. L. Tang, and S. T. Roberts, Nat. Chem. **12**(2), 137–144 (2020).
[205]E. M. Gholizadeh, S. K. K. Prasad, Z. L. Teh, T. Ishwara, S. Norman, A. J. Petty, J. H. Cole, S. Cheong, R. D. Tilley, J. E. Anthony, S. Huang, and T. W. Schmidt, Nat. Photonics **14**(9), 585–590 (2020).
[206]J. De Roo, Z. Huang, N. J. Schuster, L. S. Hamachi, D. N. Congreve, Z. Xu, P. Xia, D. A. Fishman, T. Lian, J. S. Owen, and M. L. Tang, Chem. Mater. **32**(4), 1461–1466 (2020).
[207]R. Lai and K. Wu, J. Chem. Phys. **153**(11), 114701 (2020).
[208]R. Lai, Y. Sang, Y. Zhao, and K. Wu, J. Am. Chem. Soc. **142**(47), 19825–19829 (2020).
[209]S. He, R. Lai, Q. Jiang, Y. Han, X. Luo, Y. Tian, X. Liu, and K. Wu, Angew. Chem. Int. Ed. **59**(40), 17726–17731 (2020).
[210]E. M. Rigsby, T. Miyashita, P. Jaimes, D. A. Fishman, and M. L. Tang, J. Chem. Phys. **153**(11), 114702 (2020).
[211]D. Beery, J. P. Wheeler, A. Arcidiacono, and K. Hanson, ACS Appl. Energy Mater. **3**(1), 29–37 (2020).
[212]N. Tripathi, M. Ando, T. Akai, and K. Kamada, ACS Appl. Nano Mater. **4**(9), 9680–9688 (2021).
[213]Z. A. VanOrman, C. R. Conti, G. F. Strouse, and L. Nienhaus, Chem. Mater. **33**(1), 452–458 (2021).
[214]L. Hou, A. Olesund, S. Thurakkal, X. Zhang, and B. Albinsson, Adv. Funct. Mater. **31**(47), 2106198 (2021).
[215]M. Koharagi, N. Harada, K. Okumura, J. Miyano, S. Hisamitsu, N. Kimizuka, and N. Yanai, Nanoscale **13**(47), 19890–19893 (2021).
[216]P. Xia, J. Schwan, T. W. Dugger, L. Mangolini, and M. L. Tang, Adv. Opt. Mater. **9**(17), 2100453 (2021).
[217]X. Lin, Z. Chen, Y. Han, C. Nie, P. Xia, S. He, J. Li, and K. Wu, ACS Energy Lett. **7**(3), 914–919 (2022).
[218]S. He, Y. Han, J. Guo, and K. Wu, J. Phys. Chem. Lett. **13**(7), 1713–1718 (2022).
[219]C. Wohnhaas, A. Turshatov, V. Mailänder, S. Lorenz, S. Baluschev, T. Miteva, and K. Landfester, Macromol. Biosci. **11**(6), 772–778 (2011).
[220]Q. Liu, T. Yang, W. Feng, and F. Li, J. Am. Chem. Soc. **134**(11), 5390–5397 (2012).
[221]Q. Liu, B. Yin, T. Yang, Y. Yang, Z. Shen, P. Yao, and F. Li, J. Am. Chem. Soc. **135**(13), 5029–5037 (2013).
[222]C. Wohnhaas, V. Mailänder, M. Dröge, M. A. Filatov, D. Busko, Y. Avlasevich, S. Baluschev, T. Miteva, K. Landfester, and A. Turshatov, Macromol. Biosci. **13**(10), 1422–1430 (2013).
[223]S. Mattiello, A. Monguzzi, J. Pedrini, M. Sassi, C. Villa, Y. Torrente, R. Marotta, F. Meinardi, and L. Beverina, Adv. Funct. Mater. **26**(46), 8447–8454 (2016).
[224]O. S. Kwon, H. S. Song, J. Conde, H.-I. Kim, N. Artzi, and J.-H. Kim, ACS Nano **10**(1), 1512–1521 (2016).
[225]Q. Liu, W. Wang, C. Zhan, T. Yang, and D. S. Kohane, Nano Lett. **16**(7), 4516–4520 (2016).
[226]L. Huang, Y. Zhao, H. Zhang, K. Huang, J. Yang, and G. Han, Angew. Chem. Int. Ed. **56**(46), 14400–14404 (2017).
[227]S. H. C. Askes, A. Bahreman, and S. Bonnet, Angew. Chem. Int. Ed. **53**(4), 1029–1033 (2014).
[228]B. Tian, Q. Wang, Q. Su, W. Feng, and F. Li, Biomaterials **112**, 10–19 (2017).

[229]M. Xu, X. Zou, Q. Su, W. Yuan, C. Cao, Q. Wang, X. Zhu, W. Feng, and F. Li, Nat. Commun. **9**(1), 2698 (2018).
[230]Y. Zuo, M. Tian, J. Sun, T. Yang, Y. Zhang, and W. Lin, Anal. Chem. **90**(24), 14602–14609 (2018).
[231]Z.-S. Yang, Y. Ning, H.-Y. Yin, and J.-L. Zhang, Inorg. Chem. Front. **5**(9), 2291–2299 (2018).
[232]D. Asthana, S. Hisamitsu, M.-A. Morikawa, P. Duan, T. Nakashima, T. Kawai, N. Yanai, and N. Kimizuka, Org. Mater. **1**(01), 043–049 (2019).
[233]Y. Sasaki, M. Oshikawa, P. Bharmoria, H. Kouno, A. Hayashi-Takagi, M. Sato, I. Ajioka, N. Yanai, and N. Kimizuka, Angew. Chem. Int. Ed. **58**(49), 17827–17833 (2019).
[234]H.-L. Lee, J. H. Park, H.-S. Choe, M.-S. Lee, J.-M. Park, N. Harada, Y. Sasaki, N. Yanai, N. Kimizuka, J. Zhu, S. H. Bhang, and J.-H. Kim, ACS Appl. Mater. Interfaces **11**(30), 26571–26580 (2019).
[235]Q. Wang, M. Xu, W. Feng, and F. Li, J. Lumin. **218**, 116837 (2020).
[236]R. Meir, T. Hirschhorn, S. Kim, K. J. Fallon, E. M. Churchill, D. Wu, H. W. Yang, B. R. Stockwell, and L. M. Campos, Adv. Funct. Mater. **31**(31), 2010907 (2021).
[237]B. Iyisan, R. Thiramanas, N. Nazarova, Y. Avlasevich, V. Mailänder, S. Baluschev, and K. Landfester, Biomacromolecules **21**(11), 4469–4478 (2020).
[238]L. Huang, L. Zeng, Y. Chen, N. Yu, L. Wang, K. Huang, Y. Zhao, and G. Han, Nat. Commun. **12**(1), 122 (2021).
[239]L. Li, C. Zhang, L. Xu, C. Ye, S. Chen, X. Wang, and Y. Song, Angew. Chem. Int. Ed. **60**(51), 26725–26733 (2021).
[240]O. Vepris, C. Eich, Y. Feng, G. Fuentes, H. Zhang, E. L. Kaijzel, and L. J. Cruz, Biomedicines **10**(5), 1070 (2022).
[241]A. Turshatov, D. Busko, S. Baluschev, T. Miteva, and K. Landfester, New J. Phys. **13**(8), 083035 (2011).
[242]J.-H. Kim and J.-H. Kim, J. Am. Chem. Soc. **134**(42), 17478–17481 (2012).
[243]S. Mutsamwira, E. W. Ainscough, A. C. Partridge, P. J. Derrick, and V. V. Filichev, J. Phys. Chem. B **119**(44), 14045–14052 (2015).
[244]K. Katta, D. Busko, Y. Avlasevich, R. Muñoz-Espí, S. Baluschev, and K. Landfester, Macromol. Rapid Commun. **36**(11), 1084–1088 (2015).
[245]J.-H. Kim and J.-H. Kim, ACS Photonics **2**(5), 633–638 (2015).
[246]D. C. Thévenaz, A. Monguzzi, D. Vanhecke, R. Vadrucci, F. Meinardi, Y. C. Simon, and C. Weder, Mater. Horiz. **3**(6), 602–607 (2016).
[247]Y. Tian, J. Li, L. Zhao, X. Zhang, A. Wang, H. Jian, S. Bai, and X. Yan, Biomater. Sci. **8**(11), 3072–3077 (2020).
[248]H.-C. Chen, C.-Y. Hung, K.-H. Wang, H.-L. Chen, W. S. Fann, F.-C. Chien, P. Chen, T. J. Chow, C.-P. Hsu, and S.-S. Sun, Chem. Commun. **2009**(27), 4064–4066.
[249]T. N. Singh-Rachford and F. N. Castellano, J. Phys. Chem. A **113**(20), 5912–5917 (2009).
[250]J.-H. Olivier, Y. Bai, H. Uh, H. Yoo, M. J. Therien, and F. N. Castellano, J. Phys. Chem. A **119**(22), 5642–5649 (2015).
[251]Y. Sasaki, S. Amemori, H. Kouno, N. Yanai, and N. Kimizuka, J. Mater. Chem. C **5**(21), 5063–5067 (2017).
[252]Z. Wang and J. Zhao, Org. Lett. **19**(17), 4492–4495 (2017).
[253]N. Nishimura, V. Gray, J. R. Allardice, Z. Zhang, A. Pershin, D. Beljonne, and A. Rao, ACS Mater. Lett. **1**(6), 660–664 (2019).
[254]H.-L. Lee, M.-S. Lee, H. Park, W.-S. Han, and J.-H. Kim, Korean J. Chem. Eng. **36**(11), 1791–1798 (2019).
[255]A. Mahammed, K. Chen, J. Vestfrid, J. Zhao, and Z. Gross, Chem. Sci. **10**(29), 7091–7103 (2019).
[256]Y. Dong, B. Dick, and J. Zhao, Org. Lett. **22**(14), 5535–5539 (2020).
[257]R. Haruki, Y. Sasaki, K. Masutani, N. Yanai, and N. Kimizuka, Chem. Commun. **56**(51), 7017–7020 (2020).
[258]S. R. Pristash, K. L. Corp, E. J. Rabe, and C. W. Schlenker, ACS Appl. Energy Mater. **3**(1), 19–28 (2020).
[259]B. Joarder, A. Mallick, Y. Sasaki, M. Kinoshita, R. Haruki, Y. Kawashima, N. Yanai, and N. Kimizuka, ChemNanoMat **6**(6), 916–919 (2020).
[260]Y. Wei, Y. Li, M. Zheng, X. Zhou, Y. Zou, and C. Yang, Adv. Opt. Mater. **8**(9), 1902157 (2020).
[261]Y. Wei, Y. Li, Z. Li, X. Xu, X. Cao, X. Zhou, and C. Yang, Inorg. Chem. **60**(24), 19001–19008 (2021).
[262]W. Yin, T. Yu, J. Chen, R. Hu, G. Yang, Y. Zeng, and Y. Li, ACS Appl. Mater. Interfaces **13**(48), 57481–57488 (2021).
[263]A. Olesund, J. Johnsson, F. Edhborg, S. Ghasemi, K. Moth-Poulsen, and B. Albinsson, J. Am. Chem. Soc. **144**(8), 3706–3716 (2022).
[264]T. J. B. Zähringer, M.-S. Bertrams, and C. Kerzig, J. Mater. Chem. C **10**(12), 4568–4573 (2022).
[265]M. Uji, N. Harada, N. Kimizuka, M. Saigo, K. Miyata, K. Onda, and N. Yanai, J. Mater. Chem. C **10**(12), 4558–4562 (2022).
[266]Y. Wei, K. Pan, X. Cao, Y. Li, X. Zhou, and C. Yang, "Multiple resonance thermally activated delayed fluorescence sensitizers enable green-to-violet photon upconversion: Application in photochemical transformations," CCS Chem. (published online 2022).